The Tetraspanin Protein Peripherin-2 Forms a Complex with Melanoregulin, a Putative Membrane Fusion Regulator†

Kathleen Boesze-Battaglia,*,‡ Hongman Song,§ Maxim Sokolov,§,|| Concepcion Lillo,⊥ Lisa Pankoski-Walker,@ Cheryl Gretzula,‡ Bridget Gallagher,@ Rivka A. Rachel,# Nancy A. Jenkins,# Neal G. Copeland,# Francine Morris,‡ Jerry Jacob,‡ Philip Yeagle,+ David S. Williams,⊥ and Monika Damek-Poprawa‡

Departments of Biochemistry and Pathology, School of Dental Medicine, University of Pennsylvania, Philadelphia, Pennsylvania 19104, Department of Biochemistry and Molecular Pharmacology, West Virginia University Health Sciences Center, Morgantown, West Virginia 26506, Department of Ophthalmology, West Virginia University Eye Institute, Morgantown, West Virginia 26506, Department of Pharmacology, University of California at San Diego School of Medicine, La Jolla, California 92093, Mouse Cancer Genetics Program, National Cancer Institute, Frederick, Maryland 21702, and Department of Molecular and Cell Biology, University of Connecticut, Storrs, Connecticut 06269

Received July 19, 2006; Revised Manuscript Received November 17, 2006

ABSTRACT: Peripherin-2, the product of the *rds* gene, is a tetraspanin protein. In this study, we show that peripherin-2 forms a complex with melanoregulin (MREG), the product of the *Mreg* locus. Genetic studies suggest that MREG is involved in organelle biogenesis. In this study, we explore the role of this protein in processes associated with the formation of disk membranes, specialized organelles of photoreceptor rod cells. MREG antibodies were generated and found to be immunoreactive with a 28 kDa protein in retinal extracts, bovine OS, ARPE-19 cells, and rat RPE. MREG colocalized with peripherin-2 in WT (CB6F1/J) and in rds+/− retinas. Western blots of serial tangential sections confirmed the close association of these two proteins within the IS and basal outer segment of rods. Immunoprecipitation (IP) of OS extracts showed formation of a complex between MREG and peripherin-2−ROM-1 hetero-oligomers. This interaction was confirmed with pulldown analyses in which the GST−PerCter protein selectively pulled down ^{His}−MREG and ^{His}−MREG selectively pulled down PerCter. Biacore analysis using peptide inhibitors and per-2 truncation mutant studies allowed us to map the MREG binding site on per-2 to the last five residues of the C-terminus (Gln^{341}−Gly^{346}), and kinetic data predicted a K_D of 80 nM for PerCter−MREG binding. Finally, the effect of MREG on photoreceptor specific membrane fusion was assayed using a disk−plasma membrane cell free assay. Preincubation of target membranes with MREG resulted in a dose-dependent inhibition of fusion with an IC_{50} in the submicromolar range. Collectively, these results suggest that this newly identified protein regulates peripherin-2 function.

Visual transduction, the conversion of incoming light to an electrical signal, takes place in the outer segments of the rod and cone photoreceptor cells. These highly specialized polarized post-mitotic cells are divided into a specialized inner segment region that is connected to the outer segment by a ciliary axoneme. Rod photoreceptor outer segments (OS)[1] maintain constant length and normal function through the coordination of disk morphogenesis and disk phagocytosis in a process known as photoreceptor renewal (*1*). Peripherin-2 (also known as peripherin/rds), a photoreceptor specific tetraspanin protein, plays a critical role in disk morphogenesis and stability (*2*, *3*) as well as disk shedding and phagocytosis (*4*−*6*); both processes require membrane fusion (*7*). Evidence for the essential role of this protein was established by a naturally occurring null mutation in the retinal degeneration slow (*rds*) gene. Photoreceptors of *rds* mice homozygous for the disrupted gene fail to produce OS and undergo slow degeneration (*8*). In heterozygotes, the ROS are reduced in length and irregularly arranged, consisting of whorls of membranous debris with abnormal disk shedding (*4*−*6*, *8*). The importance of peripherin-2 in OS survival was further underscored by the finding that more than 70 different mutations in peripherin-2 lead to autosomal dominant retinitis pigmentosa and macular degeneration in humans (RetNet, www.sph.uth.tmc.edu/Retnet). Interestingly, in a double-knockout mouse, the loss of both peripherin-2

† This work was supported by U.S. Public Health Service Grants EY10420 (K.B.-B.) and EY07042 (D.S.W.), Vision Core Grant P30 EY001583, and an E. Matilda Ziegler Vision Award (K.B.-B.).

* To whom correspondence should be addressed: Department of Biochemistry, School of Dental Medicine, University of Pennsylvania, 240 South 40th St., Philadelphia, PA 19104. Phone: (215) 898-9167. Fax: (215) 898-3695. E-mail: battagli@biochem.dental.upenn.edu.

‡ Department of Biochemistry, University of Pennsylvania.

§ West Virginia University Health Sciences Center.

|| West Virginia University Eye Institute.

⊥ University of California at San Diego School of Medicine.

@ Department of Pathology, University of Pennsylvania.

National Cancer Institute.

+ University of Connecticut.

[1] Abbreviations: MREG, melanoregulin; PerCter, peripherin-2 C-terminus; OS, outer segment(s); ROS, rod outer segment(s); IS, inner segment(s); RPE, retinal pigment epithelium; GARP, glutamic acid rich protein; R_{18}, *N*′-octadecylrhodamine-5-thiourea; F_{18}, *N*′-octadecylfluorescein-5-thiourea; PM, plasma membrane; *rds*, retinal degeneration slow; GST, glutathione *S*-transferase; HA, hydroxylamine; SPR, surface plasmon resonance; RSV, rim specific vesicle.

10.1021/bi061466i CCC: $37.00
Published on Web 01/18/2007

and neural retina leucine zipper (*Nrl*−/−) transcription factor results in altered disk assembly within cone photoreceptors that lack normal OS lamellae. These photoreceptors were still capable of phototransduction (*9*).

As a member of the growing tetraspanin family of membrane proteins, peripherin-2 is 41% homologous in sequence with NET-7, its nearest neighbor (*10*, *11*). These tetraspanning proteins have a short N-terminus, a large hydrophilic loop (extracellular loop 2; EC2 domain) with several distinctive cysteine motifs that are necessary for the formation of functional oligomers (*12*−*18*). The EC2 domain is the site of association between peripherin-2 and ROM-1 as well as with other peripherin-2 molecules (*12*−*18*). Peripherin-2 is unique in this protein family in that it contains the largest and most functionally diverse C-terminal region. This subregion is intrinsically disordered (*11*) and contains an incisure affinity domain (*19*), a membrane fusion domain (*20*, *21*), and an OS targeting domain (*19*, *22*). Finally, peripherin-2 links the disk rim to the cGMP-gated channel of the plasma membrane through glutamic acid rich protein, GARP, thereby stabilizing OS structure (*23*). Several studies have suggested that the C-terminal domain of peripherin-2 has little structure and may belong to a family of proteins with intrinsically disordered protein domains[2,3] (*11*, *24*). Proteins belonging to this family contain structurally disordered regions that are highly conserved between species and fulfill essential biological functions, although they lack uniform secondary and tertiary structure (*25*). Structural disorder is functionally significant because it allows for increased plasticity in the regulation of multifunctional proteins (*26*). In a murine model of retinitis pigmentosa, the *rds*-307del model, the deletion of codon 307 in the peripherin-2 gene results in a gene product with an intrinsically more ordered C-terminal domain characterized by an increase in α-helical content. Retinal degeneration in this mouse is more rapid than that observed in the *rds* homozygote (*27*).

In this study, we have identified a previously unknown binding partner of peripherin-2, melanoregulin (MREG), and demonstrate that this protein inhibits membrane fusion. Melanoregulin is the product of the *Mreg* gene locus [previously known as dilute suppressor (*dsu*) or *whn*-dependent transcript 2 (*wdt2*)] and is involved in the regulation of murine coat color through an effect on the transfer of melanosome to keratinocytes (*28*−*33*). MREG suppresses the coat-color phenotype of three pigment mutations, *dilute* (*d*), *ashen* (*ash*), and *leaden* (*ln*) which encode a melanosome transport system comprised of myosin 5A (MYO5A), rab27a, and melanophilin (MLPH), respectively (*28*, *33*). MREG was positionally cloned and shown to alter the incorporation of pigment into hair through a MYO5A-independent pathway (*34*). The *Mreg* gene contains five exons, encoding a small highly charged protein composed of 214 amino acids, the sequence of which is highly conserved between humans and mice (80% shared identity) (*27*). The role of MREG in the visual system became apparent in a series of genetic studies that evaluated the interaction of a MREG loss of function mutation with various coat color mutations. In two of these mutants, ruby (ru) and ruby2 (ru^2), the absence of melanoregulin expression suppressed the ruby eye color (*31*) by increasing the apparent level of pigmentation in the choroid but not the RPE. Most recently, the effect of MREG on eye color was shown to be due to a role in regulating organelle biogenesis in the retinal pigment epithelium and choroid, the function from which the melanoregulin name is derived.[4]

Since disk membranes may be considered specialized organelles, and it is well-known that peripherin-2 is essential for disk assembly, we tested the hypothesis that MREG is essential for peripherin-2-dependent function, specifically fusion. The hypothesis that MREG participates in processes requiring fusion is consistent with its effect on melanosome transfer and pigment incorporation (*35*). In melanocytes, the loss of MREG is postulated to alter melanosome phagocytosis, a process requiring fusion events (*34*). In this study, we provide evidence that MREG colocalizes with peripherin-2 *in vivo* in subcellular domains involved in vesicle trafficking and disk morphogenesis (IS and basal OS). Moreover, immunoprecipitation, pulldown, and surface plasmon resonance studies show formation of a complex between MREG and peripherin-2−ROM-1 hetero-oligomers with binding of MREG restricted to the C-terminus of peripherin-2. Binding requires, at a minimum, the terminal five residues of peripherin-2, Gln^{341}−Gly^{346}. Finally, MREG inhibits disk−plasma membrane fusion in a dose-dependent manner, suggesting a functional role for this protein in OS renewal processes.

EXPERIMENTAL PROCEDURES

Materials

Rabbit polyclonal anti-FLAG antibody was purchased from Sigma (F7425), rabbit polyclonal anti-actin Ab from Santa Cruz (sc-10731), mouse monoclonal anti-sodium potassium ATPase from Affinity BioReagents (MA3-924), and anti-COX I from MitoSciences (MS404). Mouse anti-rhodopsin monoclonal antibody mAb4D2, anti-peripherin-2 mAb2B6, mAb3B6, mAb5H2, and anti-ROM-1 mAb1C6 were generous gifts from R. Molday (University of British Columbia, Vancouver, BC). Monoclonal anti-MREG antibodies were generated in our laboratory as described below. Two peptides, PP-5 and PP-3, corresponding to region within the C-terminus of bovine peripherin-2 have been described previously (*18*). PP-5 is a fusion inhibitory peptide corresponding to residues Val^{312}−Leu^{326} and PP-3 to Gln^{331}−Glu^{346}. The following cell lines were assessed for MREG protein expression levels: RBL-2H3 chemically induced rat basophils (ATCC, CRL-2256), mIMCD-3 mouse inner medullary collecting duct cells (ATCC, CRL-2123), ARPE-19 human retinal pigmented epithelium (ATCC, CRL-2302), RPE-J rat retinal pigmented epithelium (ATCC, CRL-2240), and primary cell cultures derived from mouse [MNT-1 (*36*) and melan-c (*37*)].

[2] Edrington, V. T. C., Lapointe, R., Yeagle, P. L., Gretzula, C. A., and Boesze-Battaglia, K. (2006) Peripherin-2: An intracellular analogy to viral fusion proteins, *Biochemistry* (submitted for publication).

[3] Edrington, V. T. C., Yeagle, P. L., Gretzula, C. A., and Boesze-Battaglia, K. (2006) Calcium dependant association of calmodulin with the C-terminal domain of the tetraspanin protein peripherin/rds, *Biochemistry* (submitted for publication).

[4] Rachel, R. A., Nagashima, K., Lillo, C., O'Sullivan, N., Marigo, V., Boesze-Battaglia, K., Williams, D. S., Copeland, N. G., and Jenkins, N. A. (2006) Melanoregulin, product of the dsu locus, links the BLOC-pathway and Oa1 in organelle biogenesis, (submitted for publication).

Table 1: Primers Used in the Generation of the Bovine Peripherin-2 and ROM-1 Constructs[a]

mutant	primer	sequence
PerCter scrambled helix	P1 (F)	TGGAGAAGAGCGTGCCGGAGGCCTGGGGGGCCACTCTGGAGAGTGTGAA
	P2 (R)	CTCCGGCACGCTCTTCTCCAGAAGCCAGCC
	P3 (F)	GTGTGAAGAAGCTGGGCAAGGACAACTACGTGCTAGCCGAGGGCGAG
	P4 (R)	CTTGCCCAGCTTCTTCACACTCTCCAGAGT
ROM-1Cter	P5 (F)	ATTAGGATCCCGGTACCTGCAGACAGCAC
	P6 (R)	ATTAGGATCCTCACTAGGCCTCAGGCAGACACTC
PerNter	P7 (F)	ACAAGGATCCATGGCGCTGCTGAAAGTCAAATTTGACCA
	P8 (R)	ATTAGGATCCTCAGCCTGCCGCCGGGGC

[a] Forward (F) and reverse (R) primers are given.

Methods

Expression and Purification of GST−Polypeptide Constructs and Hexahistidine-Tagged MREG ($^{His-}$MREG). The GST−peripherin-2 fusion construct included the full-length peripherin-2 C-terminus (Arg^{284}−Gly^{346}, GST−PerCter). In addition, GST−peripherin-2 C-terminal substitution mutants [PerCter scrambled helix, GST−peripherin-2 N-terminus, and the GST−ROM-1 C-terminal construct with the full-length ROM-1 C-terminus (Arg^{288}−Ala^{351})] were prepared. PerCter scrambled helix was obtained using a GeneTailor Mutagenesis System (Invitrogen) with the specific primers (Table 1), according to the manufacturer's protocol. The generation of the GST−polypeptide constructs as well as the expression and purification of these fusion proteins have been described previously (*24*). Briefly, *Escherichia coli* BL21(DE3) cells transformed with GST−polypetide constructs in pGEX-2T vector (*24*, *38*) were grown in LB medium containing 50 μg/mL ampicillin. Cells were harvested 2 h after induction with 0.1 mM isopropyl β-D-thiogalactopyranoside (IPTG), spun down, washed in PBS, and sonicated in the presence of 35 mM octyl glucopyranoside (OG) in PBS (pH 7.2). Cellular debris was removed by centrifugation, and the GST−polypeptide constructs were purified on a GST affinity column (Amersham Biosciences) and either cleaved with 400 units of thrombin (10 units of thrombin/mg of protein) for use in surface plasmon resonance (SPR) studies or used as an intact fusion protein in GST pulldown assays. The GST−EC2 protein contains a region encompassing Phe^{120}−Asn^{256} and was a generous gift from M. Naash (*39*).

To generate an MREG fusion protein, *Mreg* cDNA was cloned into a pIVEX 2.4 vector with an N-terminal hexahistidine tag, and the protein was expressed *in vitro* using a Rapid Translation System RTS 500 Proteomaster *E. coli* HY Kit (Roche), according to the manufacturer's protocol. Coupled transcription−translation reactions were initiated with the addition of 20 μg of *Mreg* construct in a total volume of 1 mL for 24 h at 30 °C. $^{His-}$MREG was purified on chelating columns using the ÄTKA FPLC system (Amersham Biosciences). Briefly, columns were loaded with 2.5 mL of 0.1 M $NiSO_4$, washed with 5 mL of dH_2O and the product of each RTS reaction mixed with 4 mL of binding buffer [0.02 M sodium phosphate, 0.5 M sodium chloride, 20 mM imidazole, 35 mM OG, and 8 M urea (pH 7.4)], filtered, and loaded onto the prepared column. The flow rate was set at 1 mL/min and the maximum pressure at 0.3 MPa. The column was washed with 50 mM imidazole in elution buffer containing 0.02 M sodium phosphate, 0.5 M sodium chloride, 35 mM OG, and 8 M urea (pH 7.4) and the protein eluted with 400 mM imidazole in elution buffer. Samples were concentrated using a Centricon filter (Millipore) with a molecular mass cutoff of 10 kDa and dialyzed in six changes of PBS containing decreasing amounts of urea (4, 2, 1, and 0.5 M and 2 × no urea). The purity of $^{His-}$MREG was confirmed via 10% SDS−PAGE under reducing conditions. Gels were stained using the SilverQuest Silver Staining kit (Invitrogen), according to the manufacturer's protocol, or transferred and immunoblotted. Blots were probed with a 1:1000 dilution of either anti-MREG mAb165 or mAb126, followed by a 1:1000 dilution of sheep anti-mouse HRP-conjugated secondary antibody (Amersham Biosciences).

Table 2: Primers Used in the Construction of the Peripherin-2 C-Terminal Deletion Mutants[a]

mutant	primer	sequence	PCR product size (bp)
M1	P1 (F)	AATATCTAGATCATGCCGCCGGGGCCT	189
	P2 (R)	GAGCGGATCCCGCTACCTGCACAC	
M2	P3 (F)	GACGTCTAGATCACGCCGGGGCCT	186
	P4 (R)	GAGCGGATCCCGCTACCTGCACAC	
M3	P5 (F)	GAGCTCTAGATCACGGGGCCTGGCCT	183
	P6 (R)	GAGCGGATCCCGCTACCTGCACAC	
M4	P7 (F)	GATCTCTAGATCAGGCCTGGCCTGCGT	180
	P8 (R)	GAGCGGATCCCGCTACCTGCACAC	
M5	P9 (F)	GAGGTCTAGATCACTGGCCTGCGTCCTC	177
	P10 (R)	GAGCGGATCCCGCTACCTGCACAC	
M6	P11 (F)	GAGGTCTAGATCAGCCTGCGTCCTCGC	174
	P12 (R)	GAGCGGATCCCGCTACCTGCACAC	
M7	P13 (F)	GAGGTCTAGATCATGCGTCCTCGCCCT	171
	P14 (R)	GAGCGGATCCCGCTACCTGCACAC	

[a] Forward (F) and reverse (R) primers are given.

Construction and Expression of Plasmids Containing Deletion Mutations of the Peripherin-2 Gene. A construct containing ^{His}PerCter and a series of peripherin-2 C-terminal deletion mutants, removing designated sequential amino acids, ^{His}PerCter$^{\Delta 346}$, ^{His}PerCter$^{\Delta 345-346}$, ^{His}PerCter$^{\Delta 344-346}$, ^{His}PerCter$^{\Delta 343-346}$, and ^{His}PerCter$^{\Delta 342-346}$, were generated. Each construct contained a RBS site and a T7 promoter upstream of the respective gene and incorporated a hexahistidine N-terminal tag as well as an Xpress epitope. cDNA sequences encoding the deletion mutants were obtained by polymerase chain reaction (PCR) using the primers listed in Table 2. Each resulting PCR fragment was inserted into the multiple cloning sites of the pcDNA3.1 expression vector (Invitrogen), and the plasmids were transformed into *E. coli* JM109 cells. Transformed JM109 cells were grown in 1 L of Luria Broth (LB) and utilized to purify the recombinant plasmids for expression in MDCK cells as described previously (*40*). The authenticity of all constructs was confirmed by sequence analysis.

Generation of Anti-MREG Monoclonal Antibodies. A panel of anti-MREG monoclonal antibodies was generated

for use in these studies. Briefly, recombinant $^{His-}$MREG was expressed *in vitro* and purified by nickel affinity chromatography (*41*) as described above. Anti-MREG mAbs were generated as previously described (*42*). Briefly, Balb/c mice (Charles River Labs, Wilmington, MA), 10−12 weeks old, were immunized by IP injection with 10−20 μg of $^{His-}$MREG on days 0, 10, 20, and 30 and allowed to rest for 30 days. Three days prior to fusion, the animals received 10 μg of peptide intravenously. Splenocytes were fused to Sp2/0-Ag14 myeloma cells in the presence of 50% polyethylene glycol (Kodak 1450). The cells were then dispersed in Kennett's HY medium containing 20% FBS, glutamine, oxaloacetate, pyruvate, hypoxanthine, and azaserine and fed 7 days later in medium lacking azaserine. Clones were visible 7−9 days after fusion and were first screened with a $^{His-}$MREG ELISA. All mAbs were further screened by dot blots and Western blots using purified $^{His-}$MREG as well as by immunofluorescence to determine which antibodies could recognize MREG *in vivo*. Two of these antibodies, anti-mouse mAb126 and mAb165, were further characterized and used in these studies. These antibodies are essentially monospecific and recognize ^{His}-MREG, as well as a 28 kDa band corresponding to MREG in bovine ROS and human RPE in Western blots. The distribution of MREG in the retina detected by anti-MREG mAb126 and mAb165 was similar to that observed with AP-33 (affinity-purified polyclonal antibody) generated by J. Hammer (*34*).

Hydroxylamine (HA) Treatment of Bovine ROS. Dark-adapted bovine retinas (Lawson, Lincoln, NE) were homogenized and rod outer segments (ROS) isolated by differential centrifugation followed by discontinuous sucrose density gradient separation (*43*). All procedures were carried out under dim red light. Purified ROS (at 3 mg/mL total protein) were incubated for 30 min at 37 °C with 1 M hydroxylamine (HA) in 1 M Tris-HCl buffer (pH 7.0) (at a ratio of 50 μL of ROS to 30 μL of HA) (*44*). HA-treated samples were centrifuged at top speed for 5 min to separate proteins that dissociated from the membrane fraction. Supernatant containing the dissociated proteins was collected and the pellet resuspended in 30 μL of 10 mM HEPES (pH 7.4). Both fractions were subjected to 12% SDS−PAGE under reducing conditions and immunoblotted (*45*). Western blots were probed with a 1:1000 dilution of mouse monoclonal anti-MREG mAb165, followed by a 1:1000 dilution of sheep anti-mouse HRP-conjugated secondary antibody (Amersham Biosciences). Digital analysis of blots was performed using Kodak Image Station 440CF.

GST Pulldown Binding Assays. GST pulldown assays were performed essentially as described previously (*46*). Purified fusion protein was used for the pulldown assays within 24 h of the preparation and attached to BaculoGold glutathione−agarose beads (BD Biosciences), according to the manufacturer's specifications. The protein concentration was quantified with the BCA protein assay (Pierce Biotechnology). After overnight incubation at 4 °C, beads were washed, resuspended in 1 mL of 35 mM OG in PBS, and split into two tubes. Either pure GST−polypeptide constructs, bovine ROS, or the supernatant from hydroxylamine treatment of ROS (∼1 mg of total protein), prepared as described above, was added to the tubes. Following an overnight incubation, the beads were washed and proteins were eluted with 1 mL of 10 mM reduced glutathione in 50 mM Tris-HCl (pH 8.0). Samples were concentrated and proteins analyzed via 12% SDS−PAGE and Western blotting. Blots were probed with mouse monoclonal anti-peripherin-2 mAb2B6 (a generous gift from R. Molday), anti-MREG mAb165, and sheep anti-mouse HRP-conjugated secondary antibody (Amersham Biosciences).

Immunoprecipitation Studies. For immunoprecipitation (IP) studies, 300 μL of 1 mg/mL mouse monoclonal anti-MREG mAb165 antibody generated in our laboratory was bound to 400 μL of a 50% protein A−Sepharose bead slurry from the Seize X immunoprecipitation kit (Pierce Biotechnology); 300 μL of 1 mg/mL MOP-C21-purified immunoglobulin (Sigma) bound to 400 μL of protein A−Sepharose beads was used as a negative control. Protein extracts were prepared from purified ROS membranes isolated from bovine retinas by centrifugation through a sucrose density gradient as described previously (*47*). All procedures were carried out under dim red light. The resultant OS membrane preparation was solubilized in Triton X-100 and spun and the supernatant assayed in the IPs. This bovine OS protein extract was pre-adsorbed on MOP-C21 bound to protein A−Sepharose beads and subsequently incubated with either anti-MREG mAb165 or MOP-C21 antibodies along with protein A−Sepharose beads, according to the manufacturer's protocol (Pierce Biotechnology). After an overnight adsorption at 4 °C, beads were washed with 10 mM HEPES (pH 7.4) containing 300 mM NaCl and 0.02% sodium azide. Bound proteins were eluted with elution buffer included in the Seize X immunoprecipitation kit and analyzed by gel electrophoresis and immunoblotting with anti-peripherin-2 mAb2B6 or anti-ROM-1 mAb1C6.

R_{18} Fusion Assays. Bovine ROS disk and plasma membranes were prepared for fusion assays as described in detail (*48*). Vesicles enriched with peripherin-2 and ROM-1 were prepared essentially as described previously and were designated rim specific vesicles (RSV) (*20*). Fusion between R_{18}-labeled OS plasma membrane vesicles and target membranes was carried out as described previously (*49*). Briefly, ROS plasma membrane isolated using ricin-agarose as described (*50*) was labeled with 3−5 mol % (relative to phospholipid) octadecylrhodamine, R_{18}, as described previously (*48*). The R_{18}-labeled plasma membrane (R_{18}-PM, 50 μL of 1 mg/mL total phosphate) was added to 3.0 mL of the disk membrane suspension (1 mg/mL rhodopsin). The increase in R_{18} fluorescence intensity as the PM fuses with the disk membranes was measured over time. A linear increase was observed for up to 30 min at 37 °C. In the inhibition studies, disk membrane suspensions were pre-incubated with 1 nM to 10 mM $^{His-}$MREG at 37 °C for 30 min prior to the addition of R_{18}-PM and the initiation of fusion. In this study, fusion is calculated as % fusion, determined as the percent difference in the initial rate of fusion between control samples and those containing fusion inhibitor. Fusion kinetics were determined as described previously (*21*, *51*−*53*), with the lag time corresponding to the time before an increase in R_{18} fluorescence is observed indicative of membrane mixing and fusion (*49*). Non-fusion specific peptides corresponding to the N-terminus of peripherin-2 or the extradiskal loop of peripherin-2 had no effect on MREG-mediated inhibition of fusion.

Expression, Purification, and Fusion of Peripherin-2-Containing COS-7 Cell Membranes Using Resonance Energy

Transfer (RET) Fusion Assays. Procedures for the isolation and cloning of bovine $^{FLAG-}$peripherin-2 have previously been described (*54*). Primer design was based on sequences reported in refs *2* and *55*. SV40 transformed kidney fibroblast cells from the monkey *Cercopithecus aethiops* (COS-7) were grown in Dulbecco's modified essential medium (DMEM) as per ATCC (American Type Culture Collection) recommendations. The cells were routinely split 1:3 every third or fourth day. Transfections were performed using Lipofectamine PLUS reagent (Invitrogen). COS-7 cells seeded in 15 cm culture dishes (3×10^7 cells/dish) were transfected and harvested 48 h post-transfection, by scraping in 10 mL of 10 mM HEPES (pH 7.4). The cells were resuspended in 4 mL of homogenizing buffer [100 mM monobasic sodium phosphate, 1 mM DTT, 1 μg/mL leupeptin, and 2 μg/mL aprotinin (pH 7.4)], pelleted (1000 rpm for 5 min), lysed by being passed through a 26 gauge needle twice, and sonicated three times for 10 s. Intracellular membranes from transfected COS cells were isolated as described in ref *56* with slight modification (*54*). Cell lysates were layered onto a single-layer 30% sucrose gradient [30% (w/w) sucrose in homogenizing buffer] and spun at 25 000 rpm for 20 min at 4 °C in a SW28 Beckman ultracentrifuge rotor. The plasma membrane fraction was collected from the first interface and pelleted by centrifugation (50 000 rpm for 30 min at 4 °C), and membranes were resuspended in 1 mL of 10 mM HEPES (pH 7.4). Membranes were labeled with 1 mol % F_{18} (*N*′-octadecylfluorescein-5-thiourea, 1 mg/mL in ethanol) while being vortexed and incubated at 37 °C for 30 min in subdued light. Unincorporated label was removed with the addition of 500 μL of 2% BSA being incubated for 10 min at 37 °C, and labeled membranes were recovered by spinning at 50 000 rpm for 30 min at 4 °C. Pellets were resuspended in 500 μL of 10 mM HEPES (pH 7.4) for fusion.

Assessment of MREG−Peripherin-2 Subunit Binding. Surface plasmon resonance (SPR) studies were conducted on a Biacore X instrument (Biacore AB, Uppsala, Sweden) with active temperature control at 25 °C. The running buffer for the experiments consisted of 10 mM MOPS, 60 mM KCl, 30 mM NaCl, 5 mM $MgCl_2$ (pH 7.2), 3 mM EDTA, and 5 mM OG. Briefly, the flow rate was 50 μL/min, and the data collection rate was set to high. Ni^{2+} was coupled to both Fc1 and Fc2 of a NTA (nickel chelating surface) sensor chip (Biacore BR-1004-07). Both flow cells were washed, and the flow path to Fc1 was blocked and purified $^{His-}$MREG or PerCter allowed to bind to Fc2 until 2000 response units (RU) was achieved. To characterize the interaction between PerCter and MREG, the flow path was opened to include both flow cells. Protein samples at the concentrations given in the figure legends were serially diluted in the running buffer and injected. Binding of MREG and PerCter to each other was allowed to occur for 2 min, with the wash delay set for an additional 2 min to allow for a smooth dissociation curve. The chip surface was regenerated by injecting brief pulses of 0.35 M EDTA until the response signal returned to baseline. SPR data were analyzed with BIAevaluations, version 3.0, which employs global fitting. Sensorgrams were corrected for nonspecific binding by subtracting the control sensorgram (Fc1) from the polypeptide-containing surface sensorgram (Fc2). In all cases, the level of nonspecific binding was determined and found to be between 12 and 20% of the total level of binding and subtracted with the use of the Fc1 sensorgram. Model curve fitting of individual peptides was done with a 1:1 Langmuir binding model with a drifting baseline. This is the simplest model for the interaction between a receptor and a ligand; it follows the equation $A + B \leftrightarrow AB$. The rate of association (k_{on}) was measured from the forward reaction, and the dissociation rate (k_{off}) was measured from the reverse reaction. In lipid rich membrane binding experiments, the membranes bound nonspecifically to the ^{His}PerCter sensor chip. Subtracting the control sensorgram (Fc1) from the polypeptide containing surface sensorgram (Fc2) corrected for nonspecific binding. Routinely nonspecific binding accounted for 12−20% of total binding, based on RU values.

Immunostaining. Immunohistochemistry was performed on frozen sections of 4-month-old mouse retinas (*57*). The eyecups were fixed in 4% paraformaldehyde in PBS (pH 7.4) for 4 h at 4 °C, cryoprotected in 30% sucrose, and embedded in OCT. The 7 μm sections were doubly labeled with either a 1:10 dilution of mouse anti-peripherin-2 mAb5H2 (gift from R. Molday) or a 1:1000 dilution of mouse anti-sodium potassium ATPase antibody (Affinity BioReagents) followed by 7 μg/mL goat anti-mouse Alexa Fluor 647 secondary antibody (Invitrogen) and a 1:250 dilution of anti-melanoregulin mAb126 conjugated to Alexa Fluor 594 (custom-made). The negative control was incubated with the secondary antibodies only. Nuclei were visualized with DAPI. Images were captured on a Bio-Rad Radiance 2100 laser scanning confocal microscope using the same laser settings.

Immunoelectron microscopy was performed as described elsewhere (*58*). Briefly, ultrathin sections were obtained from LR White-embedded mouse (C57BL6) retinas and immunolabeled using an anti-MREG and anti-mouse secondary antibody conjugated to 6 nm gold particles. The section was doubly labeled with an anti-opsin rabbit polyclonal pAb01 and 12 nm gold particles conjugated to a secondary antibody (*59*).

Western Blot Analysis of Serial Tangential Sections of the Retina. Tangential sectioning of the retina was carried out as previously described (*60*). Eyes were harvested from 2-month-old Long Evans rats and dissected in HEPES-Ringer's solution [130 mM NaCl, 3.6 mM KCl, 2.4 mM $MgCl_2$, 1.2 mM $CaCl_2$, 0.02 mM EDTA, and 10 mM HEPES-NaOH (pH 7.4, osmolarity adjusted to 313 mosM)] under a stereomicroscope as follows. The anterior portion of the eye was cut away, and the lens was removed. The eyecup with the retina attached was cut into several pieces similar in size through the optic nerve. The eyecup fragment was transferred to the flattening chamber, where the retina was gently pulled away from the eyecup, and placed photoreceptors up onto a PVDF membrane on a glass capillary array (GCA 09/32/25/0/20 LM from BURLE Electro-Optics, Sturbridge, MA). The retina was flattened by applying gentle suction from underneath the glass capillary array, removing the entire Ringer's solution from the flattening chamber. The retina, now attached to the PVDF membrane, was additionally flattened when it was clamped between two glass slides separated by 0.5 mm thick spacers and frozen on dry ice. The cover glass and the spacers were subsequently removed, and the retina was sectioned in the Leica CM1850 Cryostat. The alignment of the retina surface with the cutting plane of the microtome knife was performed

as follows. Tissue freezing compound was applied to the specimen holder of the microtome and allowed to freeze. It was then sectioned through to create a flat surface large enough to accommodate the base slide holding the frozen retina. The base slide was then mounted to the freezing compound by addition of water drops to the sides of the glass base. The retina was trimmed to remove any folded edges, and the remaining flat surface was cut in 5 μm serial sections, each of which was thawed in 40 μL of sample buffer containing 6 M urea, 125 mM Tris-HCl (pH 6.8), 4% SDS, bromophenol blue tracking dye, and 10 mg/mL DTT. Aliquots (15 μL) were separated on a 26-well 10% Tris-HCl Criterion gel (Bio-Rad) and transferred to Immobilon FL PVDF membrane (Millipore). For the detection of rhodopsin, original samples were diluted 50 times. Western blot analysis of the protein distribution in serial sections was performed on an Odyssey Infrared Imaging System (LI-COR Biosciences) using primary mouse monoclonal antibodies against peripherin-2 (mAb3B6), melanoregulin (mAb126), rhodopsin (mAb4D2), COX I (MS404, MitoSciences), and secondary IRDye 680 goat anti-mouse antibody (LI-COR Biosciences).

RESULTS

Complexes of Melanoregulin with Peripherin-2−ROM-1 Hetero-Oligomers. In our first series of studies, we sought to determine if MREG was expressed in photoreceptor cells and to identify photoreceptor specific binding partners of MREG. To aid in these studies, we generated a series of mouse anti-MREG monoclonal antibodies as described in Methods. In these studies, we focused our analyses on a more extensive characterization of mAb165. As shown in Figure 1A, this antibody is immunoreactive, with a 28 kDa protein in human ARPE-19 cells and bovine retinal homogenates, and a slightly higher band (approximately 30 kDa) is observed in rat RPE-J cells. In addition, MREG was detected in Madin Darby Canine Kidney (MDCK) cells and mIMCD-3 mouse inner medullary collecting duct cells, two highly specialized polarized cell types. Finally, MREG was detected in Jurkat cells but was absent from RBL-2H3 chemically induced rat basophils, MNT-1 (primary mouse melanocytes), and melan-C (nonpigmented mouse melanocytes) cells under our immunoblotting conditions. Two of these antibodies, mAb126 and mAb165, detected purified MREG expressed *in vitro*, as well as bovine MREG in purified ROS preparations by Western blot analysis (Figure 1B). Immunoprecipitation studies using anti-MREG mAb165 were preformed to identify protein binding partners of MREG. Bovine OS membrane protein extracts were immunoprecipitated with anti-MREG mAb165. As shown in Figure 1C, a 33 kDa band immunoreactive with anti-ROM-1 mAb1C6 and a 34 kDa band immunoreactive with anti-peripherin-2 mAb2B6 were observed. The anti-MREG mAb126 was not found to be suitable for immunoprecipitation.

MREG Immunolocalization. We next analyzed the distribution pattern of MREG in wild-type (WT) CB6F1/J mouse retinas using mAb126. As shown in Figure 2, MREG appears to localize to the rod inner segment and distal portion of OS, the site of disk morphogenesis (panel A) as well as the RPE (panel B). RPE-associated MREG colocalizes with Na^+/K^+-ATPase, an apical marker of these cells (see the arrow in panel B, WT). Since anti-MREG mAb165 immunoprecipitated a complex containing peripherin-2, we also assessed the localization pattern of MREG in rds+/− and rds−/− mouse retinas. In 4-month-old rds+/− retinas, MREG is associated with the photoreceptor cell layer; in contrast, little MREG is observed in the OS in the rds−/− retina. Interestingly, MREG staining of the RPE in rds−/− is still observed with some punctuate colocalization with Na^+/K^+-ATPase (Figure 2B).

MREG Inhibits Fusion between Plasma Membrane and Target Membranes in a Cell Free Assay System. The immunoprecipitation studies and localization pattern of MREG suggest that this protein may play a role in peripherin-2-dependent function. Thus, we analyzed the effect of MREG on peripherin-2-associated disk−plasma membrane fusion processes using a cell free assay system (*7*, *20*, *21*). In these studies, we investigated the effect of increasing concentrations of MREG (from 1 nM to 10 mM) on fusion between purified OS plasma membrane (PM) and two different target membranes, disk membranes and peripherin-2−ROM-1 enriched vesicles (RSVs). Membrane merger was followed as an increase in fluorescence as R_{18}-labeled ROS plasma membranes (R_{18}-PM) fuse with target membranes. Fusion between R_{18}-PM and RSVs was inhibited by more than 60% upon addition of 10 mM MREG and by more than 40% when added to R_{18}-PM−disk−membrane assays (Figure 3). Addition of purified $^{His-}$MREG inhibited fusion between R_{18}-PM and disk membranes with an IC_{50} of 1.5×10^{-6} M and peripherin-2−ROM-1 enriched vesicles with an IC_{50} of 1.0×10^{-9} M. Finally, when MREG was added in combination with the peripherin-2 fusion domain specific inhibitory peptide, PP-5, fusion was almost completely abolished (data not shown). These results suggest that MREG is a potent fusion inhibitor at submicromolar levels.

The C-Terminus of Peripherin-2 Associates with Melanoregulin. The studies described above indicate that MREG interacts with full-length peripherin-2 and inhibits membrane fusion, a function associated with the C-terminus of peripherin-2. In the next series of experiments, we tested the hypothesis that the C-terminus of peripherin-2 interacts with MREG in pulldown assays. For these analyses, the C-terminus of peripherin-2 (residues Arg^{284}−Gly^{346}) was tagged with an N-terminal GST tag. The GST−peripherin-2 fusion protein (called, GST−PerCter) was expressed in *E. coli* as described previously (*24*) and when purified exhibited the predicted molecular masses, 30 kDa, for GST−PerCter (Figure 4B, lane 3) and the GST-cleaved peripherin-2 C-terminus, 8 kDa (Figure 4B, lanes 1 and 2). The purified PerCter polypeptide is biologically active. (1) It promotes membrane destabilization and membrane fusion in model systems. (2) It changes conformation in the presence of lipid vesicles (*24*). (3) It targets to the OS in transgenic *Xenopus* (*19*, *22*, *61*). Control GST−polypeptide constructs including a GST−peripherin-2 C-terminus with a scrambled amphiphilic fusion helix (GST−$PerCter^{Scr.Helix}$), C-terminal GST−EC2, and an N-terminal GST-tagged ROM-1 C-terminus (Arg^{287}−Ala^{351}) were expressed in *E. coli* (Figure 4C, lanes 4−6). Full-length MREG was tagged with an N-terminal hexahistidine $^{His-}$MREG, expressed *in vitro* using an RTS expression system, and purified to homogeneity, corresponding to a 28 kDa band as shown in Coomassie blue-stained gels in lane 1 of Figure 4C. The identity of the polypeptide was confirmed by Western blotting using

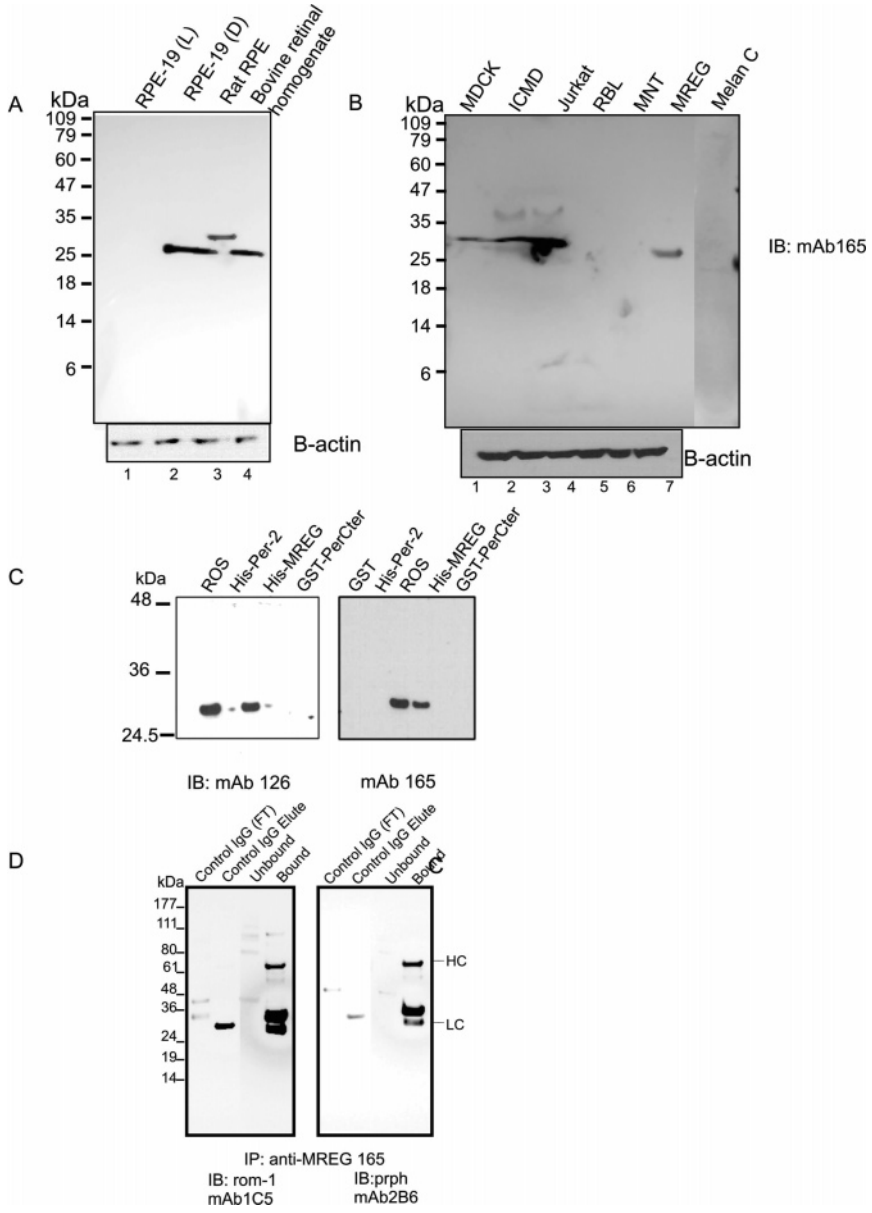

FIGURE 1: Expression of MREG and immunoprecipitation from OS extracts. (A) Western blot of human ARPE-19 cells cultured and isolated in the light, ARPE-19 (L), or in the dark, ARPE-19 (D), and rat RPE-J cells and bovine retinal homogenate immunoblotted with anti-MREG mAb165. (B) Cell lysates from the indicated cell lines were also analyzed by Western blotting using anti-MREG mAb165. (C) Western blot of purified ROS extracts, $^{His-}$MREG, and *E. coli*-expressed GST fusion proteins using anti-MREG mAb126 and anti-MREG mAb165. (D) Peripherin-2 interacts with MREG. Anti-MREG mAb165 was used to immunoprecipitate protein from ROS extracts, and the IP products were detected with anti-rom-1 mAb1C6 or anti-peripherin-2 mAb2B6 as described in Methods.

mAb165 (Figure 4C, lane 2).

In the first series of pulldown studies, $^{His-}$MREG, designated as the bait (Figure 4D), was incubated with purified GST−polypeptide constructs as the prey. A 30 kDa protein immunoreactive with anti-peripherin-2 mAb2B6 was pulled down by $^{His-}$MREG. GST alone did not interact with $^{His-}$MREG. No detectable binding with GST−PerCter$^{Scr.Helix}$, GST−EC2, or GST−ROM-1Cter was observed in these experiments (Figure 4D, lane 1). In reciprocal pulldown assays, when GST−polypeptide constructs were used as the bait (Figure 4E) and purified $^{His-}$MREG was added as prey, a 28 kDa protein immunoreactive with anti-MREG mAb165 was detected in the bait−prey complex with PerCter (Figure 4E, lane 1). In contrast, no MREG was detected if GST−PerCter$^{Scr.Helix}$, GST−EC2, or GST−ROM-1Cter was used as bait. Finally, when purified PerCter was added to the immobilized GST−PerCter as prey, no complex formation was detected, and when $^{His-}$MREG was added to $^{His-}$MREG as prey, no complex formation was detected (data not shown). No nonspecific reactivity of anti-peripherin-2 mAb2B6 to $^{His-}$MREG (Figure 4D lane 1) or anti-MREG mAb165 to PerCter was detected (data not shown). These results suggest that full-length MREG interacts with the C-terminus of peripherin-2.

Kinetics of Formation of the MREG−Peripherin-2 Complex, a Surface Plasmon Resonance (SPR) Study. The kinetics of formation of the MREG−PerCter complex was further characterized by analyzing the thermodynamic binding parameters of peptide interactions using Biacore. The Biacore is an optical biosensor which detects changes in surface plasmon resonance (SPR) in quantitatively measuring the direct interaction between biomolecules in real time without

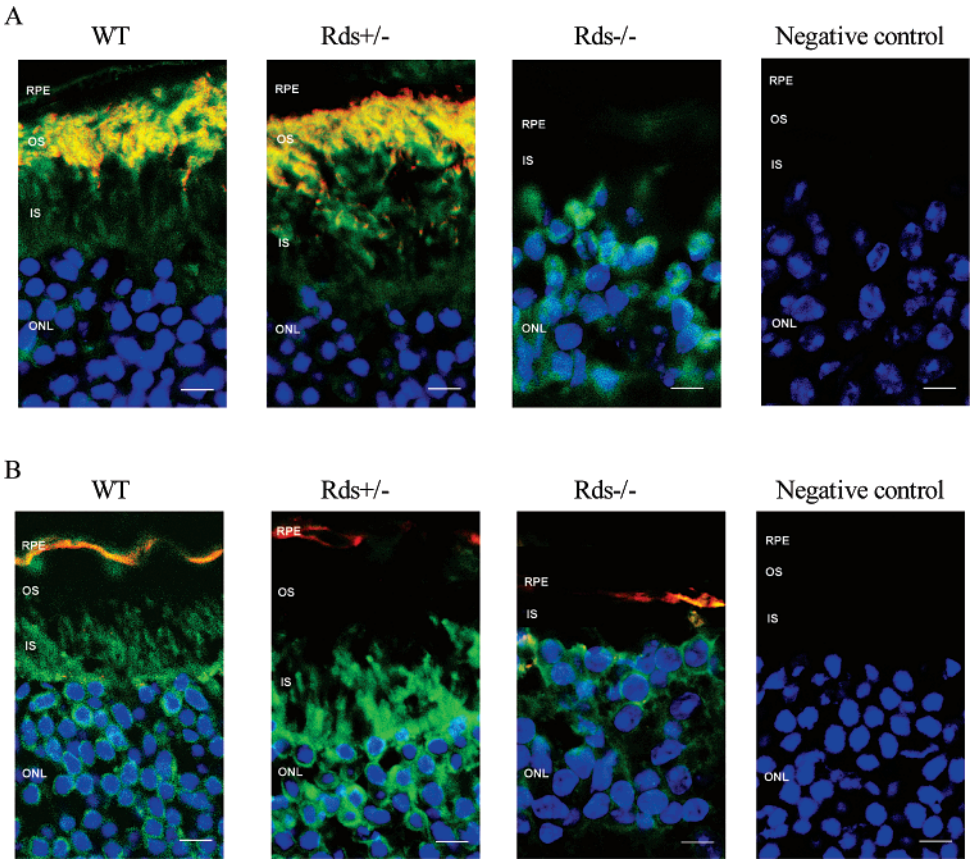

FIGURE 2: (A) Immunolocalization of MREG in mouse retinas. Sections (7 μm) of fixed 4-month-old mouse WT (CB6F1/J), *rds*+/−≪ and *rds*−/− retinas were stained with either anti-peripherin-2 mAb5H2 to mark outer segments (A) or anti-sodium potassium ATPase to detect the apical region of RPE (B) followed by anti-mouse Alexa Fluor 647 secondary antibody (colored red) and double labeled with anti-melanoregulin mAb126 conjugated to Alexa Fluor 594 (colored green). Nuclei were visualized with DAPI. Images were captured on a Bio-Rad Radiance 2100 laser scanning confocal microscope (Bio-Rad) using the same laser settings: RPE, retinal pigment epithelium; OS, outer segment; IS, inner segment; and ONL, outer nuclear layer. The scale bar is 5 μm. Arrows indicate colocalization of MREG and sodium potassium ATPase.

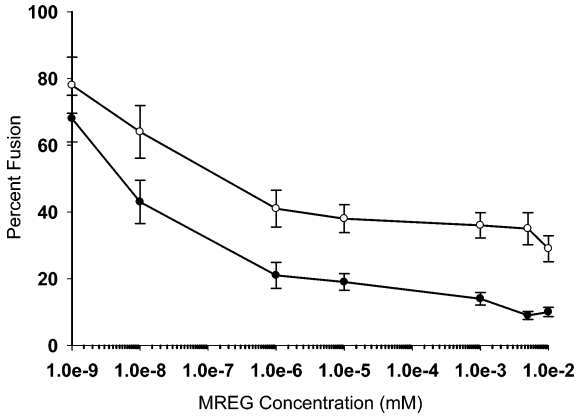

FIGURE 3: MREG inhibition of R_{18} plasma membrane−target membrane fusion. Fusion was assessed as an increase in R_{18} fluorescence over time as R_{18}PM fuses with either disk membranes preincubated with the indicated amounts of MREG at 37 °C for 30 min (○) or peripherin-2-enriched rim specific vesicles preincubated with the indicated amounts of MREG (●). The amount of fusion was measured at 37 °C as described in Methods and is presented as the percent of the total fusion. Data represent two independent experiments with fusion assays performed in triplicate.

the need for labels. In these studies, an N-terminal hexahistidine-tagged PerCter polypeptide (called ^{His}PerCter, construct shown in Figure 4A) was expressed *in vitro* using an RTS expression system and purified as described above for $^{His-}$MREG. ^{His}PerCter was coupled to a sensor chip surface [NTA (Ni^{2+})], and during the initial 50 s, a buffer baseline was established. The sample was subsequently injected and association of the sample with ^{His}PerCter followed for 2 min and dissociation of the complex followed for an additional 2 min as the sample was replaced with buffer. The data are presented as a sensorgram, which shows response units (RU) plotted as a function of time. In preliminary experiments, we determined that there was very little nonspecific binding (<10%) of the protein to the activated and blocked surface on Fc1; nonetheless, data from Fc1 were subtracted from the data from Fc2 to correct for changes in bulk refractive index and nonspecific binding to the sensor chip surface.

Figure 5A shows a group of sensorgram overlays for the binding of various components to immobilized ^{His}PerCter. The anti-peripherin-2 mAb2B6, the epitope of which corresponds to the terminal 12 residues of peripherin-2, binds to the immobilized ^{His}PerCter, suggesting that the bound polypeptide assumes a native conformation. Since the ^{His}PerCter polypeptide changes conformation upon membrane association (*24*), we wanted to determine if this conformational change resulted in measurable changes in RU. Thus, we injected three lipid rich membranes, including purified ROS membranes, OS plasma membrane, and vesicles prepared from disk lipid extracts, onto immobilized ^{His}PerCter. As shown in the sensorgrams, when purified ROS membranes were injected, an increase of >100 response units was observed (Figure 5A). This result is in contrast with

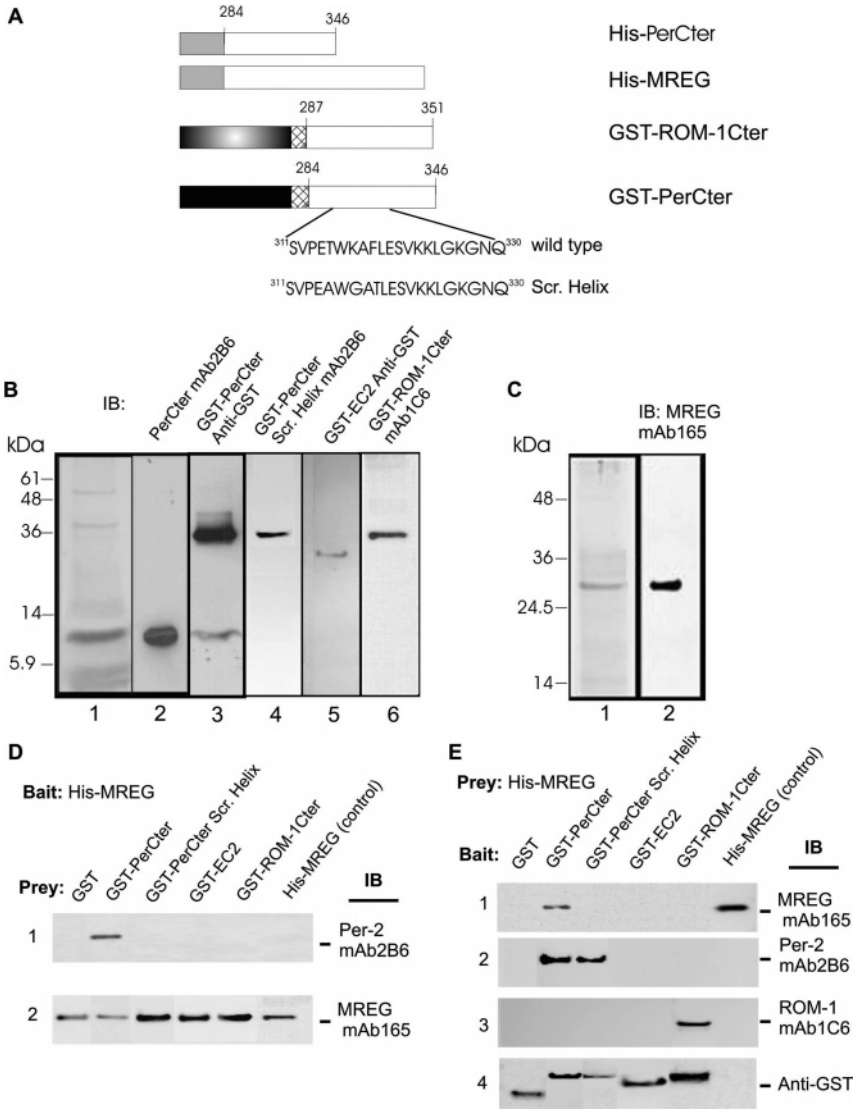

FIGURE 4: Construction, expression, and interaction of the GST−PerCter construct with MREG. (A) Schematic diagram showing the structure of fusion proteins, hexahistidine-tagged peripherin-2 C-terminus (^{His}PerCter), hexahistidine-tagged MREG ($^{His-}$MREG), and GST-tagged peripherin-2 C-terminus wild type and scrambled helix (GST−PerCter and GST−PerCter$^{Scr.Helix}$, respectively). (B) Coomasie blue-stained gel (lane 1) showing expression of purified PerCter and Western blot analysis of purified PerCter using mAb2B6 (lane 2) and GST−PerCter fusion protein using anti-GST (lane 3) as well as purified control GST−polypeptide constructs: GST−PerCter$^{Scr.Helix}$ using mAb2B6 (lane 4), GST−EC2 using anti-GST antibody (lane 5), and GST−ROM-1Cter using mAb1C6 (lane 6). (C) Coomasie blue-stained gel of purified $^{His-}$MREG (lane 1) and Western blot analysis of $^{His-}$MREG fusion protein probed with anti-MREG mAb165 (lane 2). (D) $^{His-}$MREG interacts with PerCter. The $^{His-}$MREG fusion protein attached to the Ni^{2+} resin was incubated with purified GST−polypeptide constructs at 4 °C overnight as detailed in Methods. Interaction of MREG and the purified PerCter was verified by Western blot analysis with the anti-peripherin-2 mAb2B6 (lane 1). The binding of the bait to the Ni^{2+} resin was confirmed using anti-MREG mAb165 (lane 2). (E) The GST−PerCter fusion protein interacts with $^{His-}$MREG. The GST fusion proteins attached to the glutathione resin were incubated with purified $^{His-}$MREG at 4 °C overnight as detailed in Methods. Interaction of MREG and the purified PerCter was verified by Western blot analysis with the anti-MREG mAb165 (lane 1). The binding of the GST−polypeptide constructs to the glutathione resin was confirmed using mAb2B6 (lane 2), mAb1C6 (lane 3), and anti-GST antibody (lane 4).

vesicles prepared from disk lipid extracts and plasma membrane vesicles that showed no detectable change in RUs. Collectively, these results suggest that ^{His}PerCter binds ROS membrane-associated protein(s) and that the change in RUs is not due to a conformational change in ^{His}PerCter since such a change would be expected in the presence of all three types of lipid vesicles.

Once we had established that the immobilized ^{His}PerCter assumes a native-like conformation, we injected purified MREG in 2-fold serial dilutions over the loaded sensor chip. Figure 5B shows a group of sensorgram overlays for the binding of MREG (1.2−10 μM) to immobilized ^{His}PerCter. The lines represent the best global fits to a simple Langmuir binding model with a drifting baseline, assuming that MREG was a monomer in solution (*34*). Using this model, the P_2 measures (a standard statistical measure for the closeness of fit) were all below 10, and the residuals, which correspond to the difference between actual and fitted data, are within ±5 RU, indicating a good fit (not shown). Assessment of fit is important since the on and off rates are calculated from the fitted data. Calculation of the affinity of MREG for immobilized ^{His}PerCter was (5.61 ± 1.27) × 10^{-9} M (K_D, Table 3), indicating the formation of a stable complex.

In a complementary series of studies, $^{His-}$MREG was immobilized on a sensor chip surface [NTA (Ni^{2+})] and 2-fold serial dilutions of the purified GST−PerCter polypep-

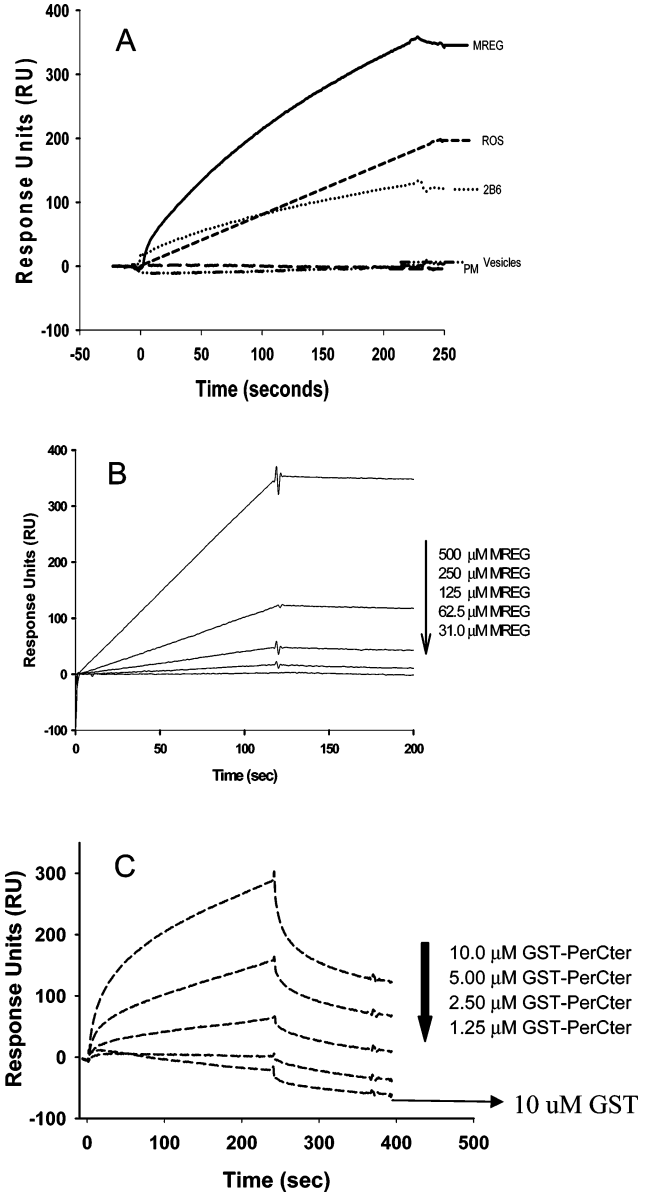

FIGURE 5: Binding of MREG to PerCter assessed by surface plasmon resonance. (A) Overlay of sensorgrams showing that immobilized peripherin-2 interacts with MREG, OS extracts, and a PerCter specific mAb, mAb2B6. PerCter does not interact with vesicles or OS PM extracts. (B) Overlay of sensorgrams showing the interaction of decreasing concentrations of MREG with immobilized PerCter. Data points were collected every 0.2 s. (C) Representative overlay of sensorgrams showing the interaction of decreasing concentrations of PerCter with immobilized MREG. The thin arrow indicates the response with just GST without peripherin-2. Data points were collected every 0.2 s.

Table 3: Kinetics and Affinity Values for Formation of the MREG−PerCter Complex

immobilized ligand	analyte	k_{on} ($\times 10^3$ s^{-1} M^{-1})	k_{off} ($\times 10^{-3}$ s^{-1})	K_D ($\times 10^{-9}$ M)
PerCter	MREG	129 ± 14.8	50.8 ± 7.25	5.61 ± 1.27
MREG	PerCter	128 ± 7.5	107 ± 2.64	80.4 ± 1.59

tide (Figure 4B, lane 3) were injected over the loaded sensor chip (Biacore). As shown in Figure 5C, GST−PerCter bound in a dose-dependent manner. GST added alone did not bind to the immobilized MREG. As indicated above, the lines represent the best global fits to a simple Langmuir binding model with a drifting baseline, assuming that PerCter was a monomer in solution (*11*, *62*). Calculation of the affinity of PerCter for immobilized $^{His-}$MREG was $(80.4 \pm 1.59) \times 10^{-9}$ M (K_D, Table 3), indicating the formation of a stable complex. Analysis of the data indicates that the binding kinetics for the formation of the complex was similar to that observed when the molecules were in the reverse orientation (K_D, Table 3).

Mapping of the MREG Binding Site to the C-Terminus of Peripherin-2. Once we established that the K_D of MREG−PerCter binding was in the nanomolar range, we proceeded to map the region of the C-terminus that interacts with MREG. In these peptide competition studies, we determined which if any of a series of overlapping C-terminal peptides (depicted in Figure 6A) inhibits complex formation using SPR. An equimolar mixture containing purified MREG and any one of the peptides (*21*) was injected onto the immobilized ^{His}PerCter. The change in RUs between formation of the MREG−^{His}PerCter complex in the presence of the individual peptides is shown in Figure 6B. Only one peptide, PP-3, inhibited binding between MREG and ^{His}PerCter, with a decrease of 60 RU. This peptide corresponds to the terminal 10 residues of peripherin-2, a region containing the mAb2B6 epitope (*2*, *63*). Analysis of the data indicates that the binding kinetics for the competitive inhibition of complex formation, K_i, of this interaction was 31×10^{-7} M. When the immobilized ^{His}PerCter was preincubated with PP-3 for 1 min prior to the addition of MREG, similar results were obtained (data not shown). In a complementary study, $^{His-}$MREG was immobilized on the chip surface and PP-3 added. Figure 6C contains a series of overlaid sensorgrams showing that addition of PerCter inhibits 50% of binding of PP-3 to $^{His-}$MREG as evidenced by the 2-fold decrease in the peptide's RUs, confirming our observation that MREG interacts with this region of PerCter.

A collective analysis of the results presented thus far predicts that removal of the MREG binding domain would affect peripherin-2-dependent fusion. This hypothesis was tested with peripherin-2 deletion mutants peripherin-$2^{\Delta 336-346}$, in which the terminal 10 residues are deleted, and peripherin-$2^{\Delta 296-346}$, in which we deleted the entire C-terminus. The full-length wild-type protein and the mutants were expressed in COS-7 cells as described previously (*54*). Peripherin-2-enriched membranes were isolated and labeled with F_{18}, and fusion with R_{18}-PM vesicles was followed over time as described in Methods using resonance energy transfer techniques. In these studies, two kinetic parameters of fusion were followed: the lag time of fusion, a time corresponding to the length of time it takes to assume a fusion competent form of peripherin-2, and the rate of fusion, an inherent measure of peripherin-2 fusogenicity. As shown in Figure 6E, the peripherin-$2^{\Delta 336-346}$ mutant had the shortest lag time, ≤ 10 s, while the full-length peripherin-2 exhibited a lag time of >10 s. Coupled with this decreased lag time, an increase in the initial rate of fusion (IRF) also was observed with the peripherin-$2^{\Delta 336-346}$ mutant (Figure 6D).

In this final series of SPR studies, we mapped the minimal binding domain of MREG to ^{His}PerCter with a series of ^{His}PerCter truncation mutants. These mutants were designed to delete the terminal seven residues of the C-terminus of peripherin-2, one at a time. ^{His}PerCter deletion mutants were

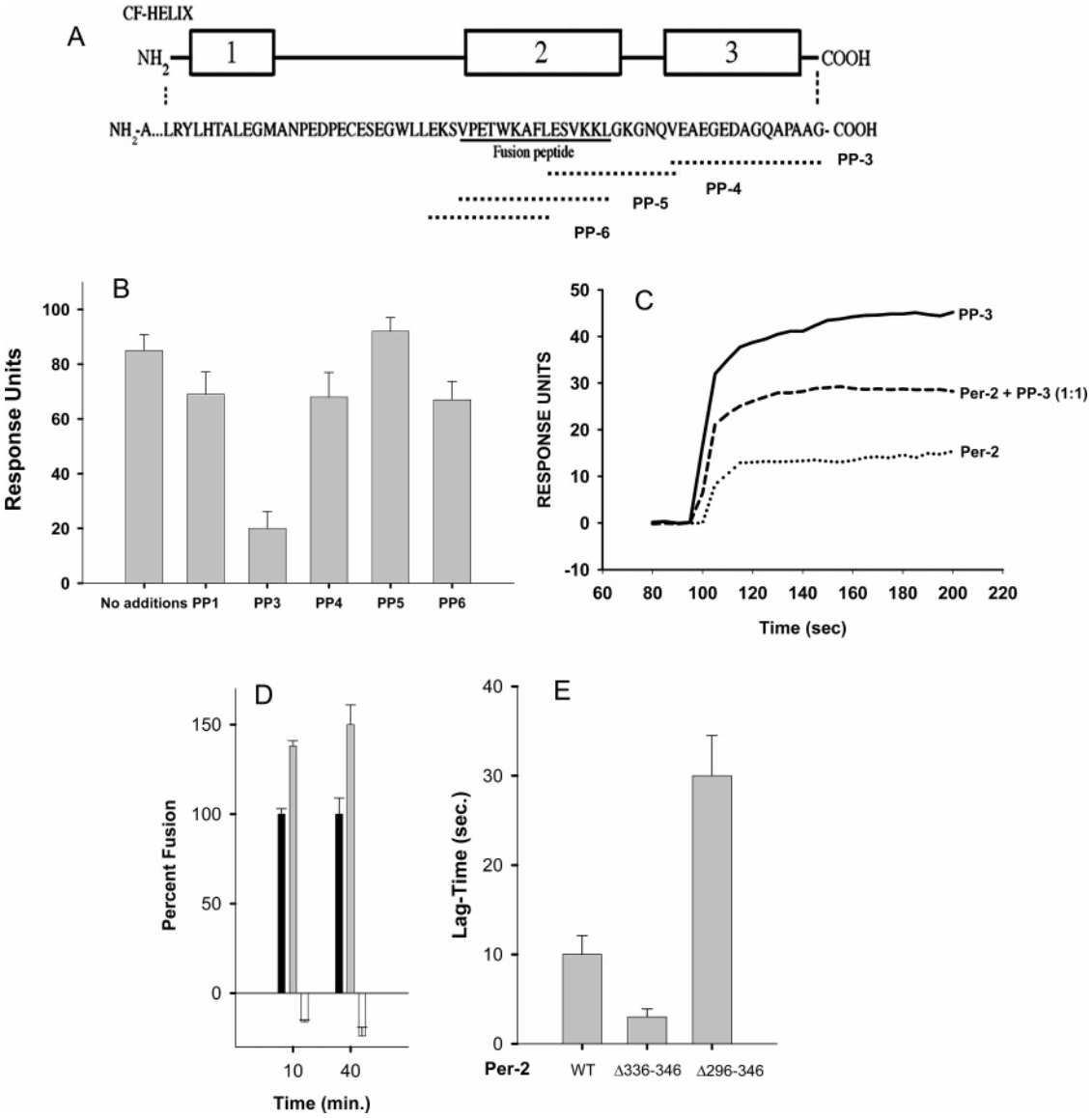

FIGURE 6: Identification of a region of PerCter that binds MREG using peptide competition studies. (A) C-Terminal domain of bovine peripherin-2 corresponding to residues 289−346. Regions 1−3 represent α-helical domains as predicted by Chou−Fasman analysis (*54*). The series of overlapping peptides used in the competition studies is given. (B) Binding of PerCter to MREG is inhibited by PP-3, a peptide corresponding to the terminal 10 residues of peripherin-2. The binding of PerCter preincubated with the indicated peptides to immobilized MREG was followed using SPR as described in Methods. RU changes upon the addition of individual peptides are shown. Data represent three independent binding studies, each of which was carried out in duplicate. (C) Representative sensorgrams of PP-3, PerCter, and an equimolar mixture of PP-3 and PerCter, binding to immobilized MREG. Fusion of R_{18} plasma membrane with target membranes containing peripherin-2 mutants. (D) Fusion between R_{18}PM and purified F_{18}-labeled COS-7 cell membranes enriched with full-length FLAG-peripherin-2 (black), FLAG-per2$\Delta^{336-346}$ (gray), or FLAG-per2$\Delta^{296-346}$ (white) was assessed as an increase in R_{18} fluorescence over time at 37 °C as described in Methods. Data represent two independent experiments with fusion assays performed in triplicate. (E) Lag time of fusion between R_{18}PM. The time prior to a linear increase in R_{18} fluorescence indicative of membrane fusion is plotted for the fusion reactions shown in panel D.

expressed *in vitro* and purified exactly like full-length ^{His}PerCter. ^{His}PerCter deletion mutants were individually immobilized on the sensor chip surface, and the binding of MREG was followed as described above. Figure 7 shows overlaid sensorgrams of the individual ^{His}PerCter deletion mutants, ^{His}PerCter$^{\Delta346}$, ^{His}PerCter$^{\Delta345-346}$, ^{His}PerCter$^{\Delta344-346}$, ^{His}PerCter$^{\Delta343-346}$, and ^{His}PerCter$^{\Delta342-346}$, and MREG. The ^{His}PerCter$^{\Delta346}$ bound to the MREG almost as well as the wild-type ^{His}PerCter. Binding of MREG to ^{His}PerCter was completely abolished upon deletion of the last five residues of the peripherin-2 C-terminus, in the PerCter$^{\Delta342-346}$ mutant. Deletion of the sixth (PerCter$^{\Delta341-346}$ mutant) and seventh (PerCter$^{\Delta340-346}$ mutant) residues yielded results similar to those for the PerCter$^{\Delta342-346}$ deletion (data not shown). Collectively, the SPR studies confirmed the *in vitro* pulldown assays showing association of ^{His}PerCter with MREG; they provided additional details about the kinetics of this process, showed high-affinity complex formation with a K_D on the order of nanomolar, and have allowed us to partially map the site of MREG−peripherin-2 interaction to the terminal five residues of ^{His}PerCter.

Membrane Affinity of Melanoregulin. Although peripherin-2 is a well-characterized membrane protein, the disposition of MREG in OS is unknown. On the basis of its localization pattern and membrane fusion inhibitory function, we hypothesized that MREG is loosely associated with ROS

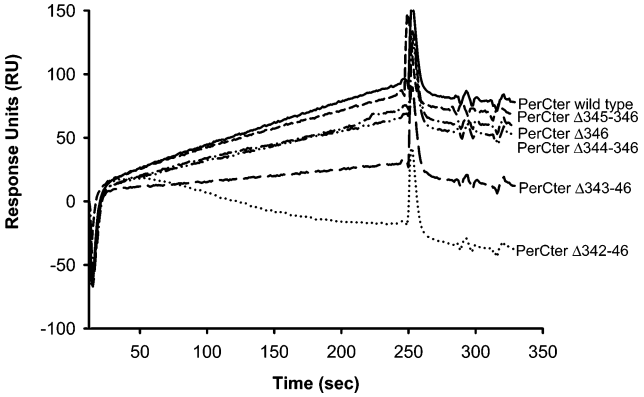

FIGURE 7: Terminal five residues of PerCter required for MREG binding. Shown is an overlay of sensorgrams showing the interaction of wild-type PerCter and five PerCter mutants, ^{His}PerCter$^{\Delta 346}$, ^{His}PerCter$^{\Delta 345-346}$, ^{His}PerCter$^{\Delta 344-346}$, ^{His}PerCter$^{\Delta 343-346}$, and ^{His}PerCter$^{\Delta 342-346}$ with immobilized MREG. Data points were collected every 0.2 s.

membranes or membrane proteins. To test this hypothesis, purified bovine ROS membranes were treated with hydroxylamine hydrochloride (HA-HCl) (*44*), allowing previously associated proteins to be released into the supernatant. As shown in Figure 8A, a 28 kDa band immunoreactive with anti-MREG mAb165 was detected in the supernatant fractions of HA-treated ROS membranes. No detectable immunoreactivity was observed in the membrane rich pellet fraction (Figure 8A, lane 2). To determine if this soluble MREG forms a complex with GST−PerCter, the supernatant fraction from HA-treated ROS was used as the prey in GST pulldown studies as described in the legend of Figure 4. As shown in Figure 8B (lane 2), GST−PerCter pulls down MREG isolated in the HA-treated ROS supernatant. No detectable MREG was associated with the GST−PerCter complex in the absence of HA (Figure 8B, lane 1).

To determine if soluble MREG affects cell-free fusion, we followed fusion between HA-treated disk membranes and R_{18}-PM (Figure 8C). Hydroxylamine-treated disk membranes had 2-fold higher initial rates of fusion than untreated disk membranes. When MREG, recovered in the HA supernatant (Figure 8A), was added back to the disk membranes, fusion inhibition was restored. Finally, when purified MREG was added to the HA-treated disk membranes (MREG-stripped membranes), inhibitory function was again restored (Figure 8C). Collectively, these results suggest that MREG functions as a fusion inhibitor *in vitro*; its mechanism of action may be regulated by its association with either the membrane through acylation or other proteins in a fusion complex. At present, studies aimed at addressing these questions are underway.

Subcellular Localization of MREG. Crucial for understanding the role of MREG in modulating peripherin-2 function is knowledge of its subcellular localization in rods. Immunostaining studies shown in Figure 2 suggest colocalization between peripherin-2 and MREG specifically within the IS and basal disk region. In this next series of studies, we analyzed the subcellular distribution of MREG using serial tangential sectioning of flat-mounted frozen retinas coupled with Western blot analysis of proteins of interest in each section. In this approach, the subcellular localization of proteins of interest in the rod is determined by comparing its distribution in the sections with the distribution of protein markers confined to specific subcellular compartments. A

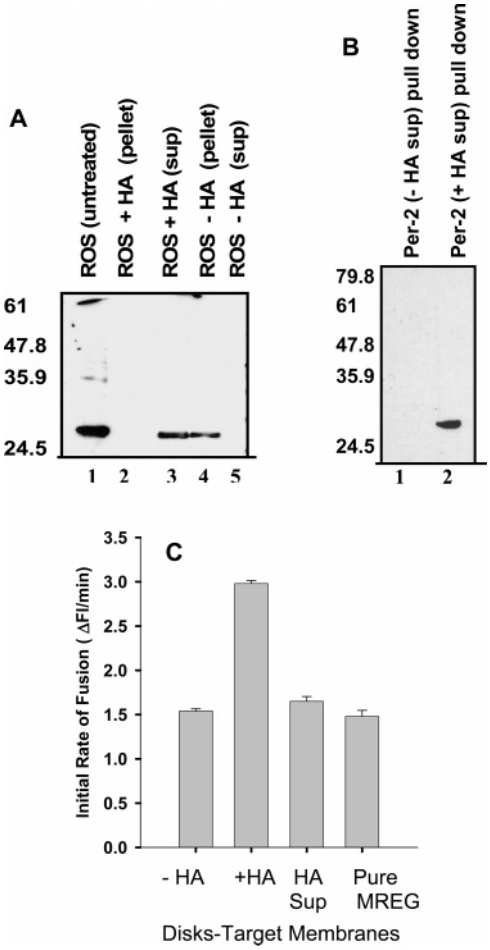

FIGURE 8: Membrane disposition of MREG in ROS membranes and association of soluble MREG with PerCter. (A) Western blot analysis of untreated ROS membranes and ROS pellets and supernatants treated with HA as indicated. Blots were probed with anti-MREG mAb165. (B) PerCter interacts with soluble MREG. The GST−PerCter fusion protein attached to the glutathione resin was incubated with either the pellet or the supernatant fraction from HA-treated ROS. Samples were incubated at 4 °C overnight as detailed in Methods. Interaction of MREG and the purified PerCter was verified by Western blot analysis with anti-MREG mAb165. (C) Fusion was assessed as an increase in R_{18} fluorescence over time as R_{18}PM was incubated with either untreated disk membranes (designated −HA), HA-treated disk membranes (designated +HA), disk membranes incubated with MREG containing HA supernatant (designated HA sup), or disk membranes preincubated with pure MREG (designated pure MREG). Fusion was assessed at 37 °C as described in detail in Methods. Data represent two independent experiments with fusion assays performed in triplicate.

representative experiment using this technique is shown Figure 9. The distribution of peripherin-2 and MREG throughout the serial sections obtained from the retina of a dark-adapted rat was compared with the distribution of the rod outer segment marker, rhodopsin, and the inner segment marker, subunit I of cytochrome *c* oxidase, COX I, a mitochondrially encoded protein present in the ellipsoid part of the inner segment densely populated with mitochondria. Our data indicate that MREG is enriched in sections corresponding to the rod inner segment (Figure 9B, sections 7−9) and basal-most disks (sections 5−7). Peripherin-2 was uniformly distributed along the length of the outer segment (sections 2−7) and also observed in MREG rich regions, including the inner segment and basal disks. Finally, the distribution of MREG within photoreceptors was further

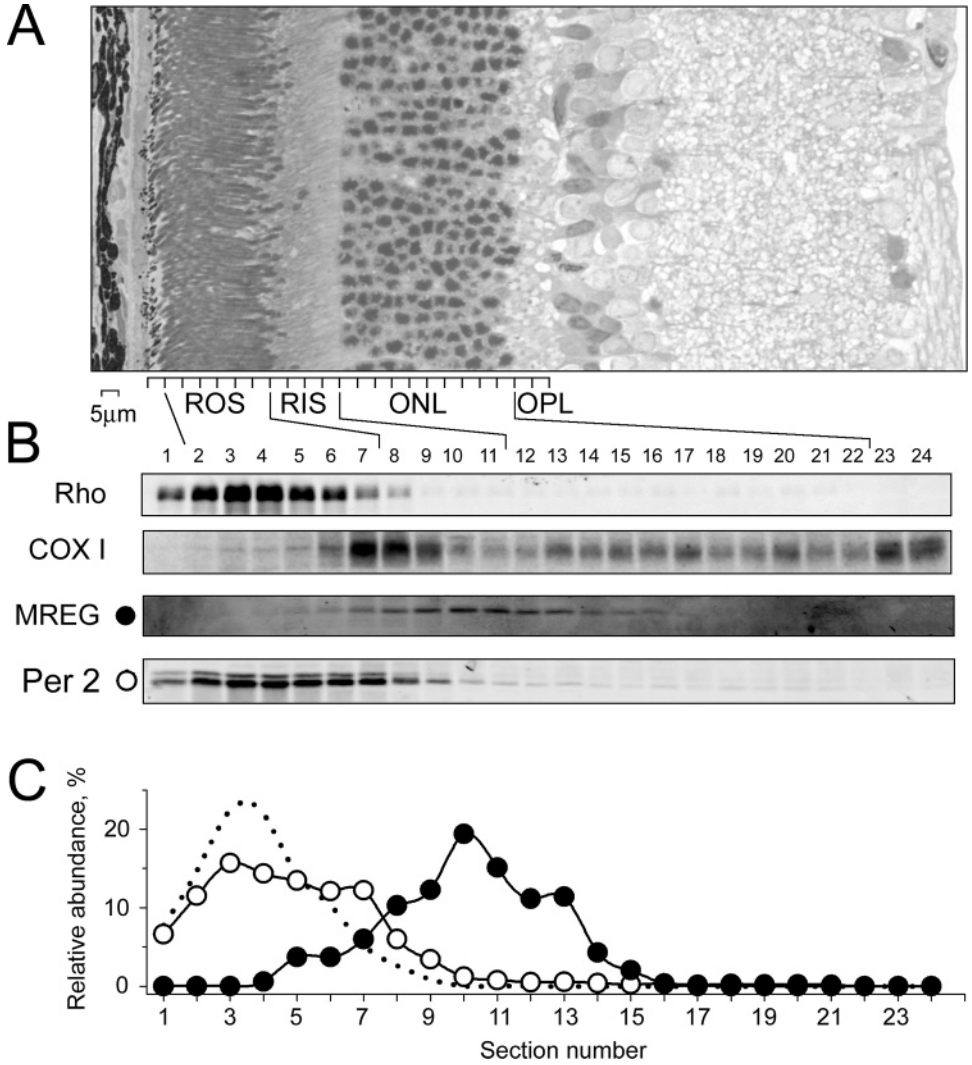

FIGURE 9: Analysis of protein distribution in the retina by Western blotting of serial tangential sections. (A) Thin rat retina cross section counterstained with toluidine blue (courtesy of A. Michaud, Massachusetts Eye and Ear Infirmary, Boston, MA). Retinal layers are as follows: ROS, rod outer segments; RIS, rod inner layer. (B) Rat retina was flat-mounted, frozen, and serially 5 μm sectioned. The protein content of each section was analyzed by Western blotting using antibodies against proteins indicated on the left of each blot. (C) Fluorescence of MREG (●) Per 2 (○) and rhodopsin (· · ·) bands in each section plotted as a percentage of a combined fluorescence in all sections. The data are taken from one of three similar experiments.

refined by immunoEM. ImmunoEM was performed with either anti-MREG mAb-126 or mAb-165; both antibodies labeled the inner segments with a similar pattern, suggestive of IS vesicle labeling with no appreciable label in the OSs (Figure 10A). Labeling with mAb165 was detected over some inner retinal cells. Double labeling with opsin antibody and either MREG antibody indicated that the MREG label did not colocalize with opsin-containing vesicles in the inner segment (Figure 10B).

DISCUSSION

The most divergent region within the tetraspanin family of proteins, the C-terminal domain, may also confer functional specificity to these proteins (*10*). The C-terminus of peripherin-2 alone has numerous unique functions in photoreceptor cells. At one level, the multifunctionality of peripherin-2 is most likely due to the formation of homo-oligomers and hetero-oligomers with ROM-1. Recent evidence suggests that functional plasticity is conferred by the intrinsically disordered nature of the C-terminus, resulting in the association of peripherin-2 with other numerous ROS proteins (*23*, *64*). Since it functionally differs from the base to the tip of the outer segment, one may expect the association of peripherin-2 with various regulatory proteins to be transient along the length of the OS.

This investigation uses a combination of GST pulldowns and surface plasmon resonance to assess formation of the peripherin-2 complex with a newly identified 28 kDa protein, melanoregulin, *in vitro* and immunoprecipitation studies to analyze complex formation *in vivo*. Collectively, these studies suggest that MREG binding requires an intact peripherin-2 C-terminus. In our studies, MREG did not appear to associate with the C-terminus of ROM-1. Biacore studies not only confirmed the formation of a MREG−peripherin-2 complex but also provided us with sensitive detection of molecular interactions in real time. The constant for binding of peripherin-2 to immobilized MREG was (80.4 $\pm$ 1.59) $\times$ 10^{-9} M, and that for the association of MREG with peripherin-2 was (5.61 $\pm$ 1.27) $\times$ 10^{-9} M. This variability in binding affinity is most likely due to the conformation of MREG on the chip. We anticipate that peripherin-2 is likely in a native conformation since periph-

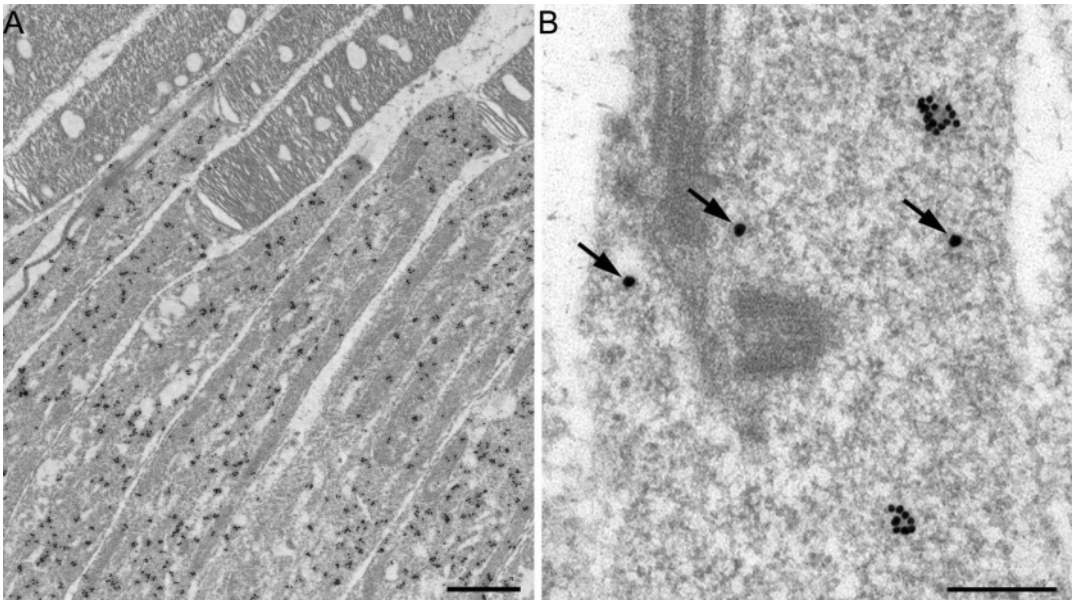

FIGURE 10: Immunogold labeling of MREG and rhodopsin in mouse photoreceptors. Ultrathin sections of LR White-embedded wild-type C57BL6 mouse retina, immunogold labeled with anti-MREG mAb126 antibody (6 nm gold particles) and anti-opsin antibody (12 nm gold particles). (A) Section labeled with the MREG antibody. Clusters of label are evident throughout the inner segments (bottom portion). The outer segments (top portion) are not labeled. The scale bar is 1 μm. (B) Higher magnification of a section double labeled with both MREG and opsin antibodies. The area shown is at the base of the cilium; the basal bodies are evident. The arrows point to single gold particles indicating opsin labeling. The opsin labeling and melanoregulin labeling do not coincide. The scale bar is 300 nm.

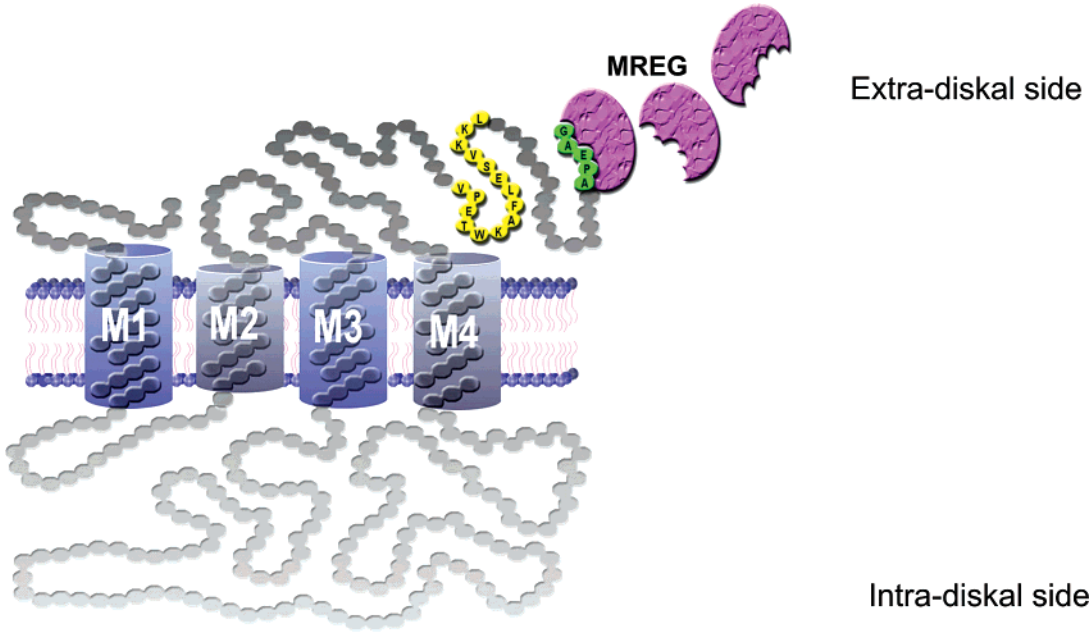

FIGURE 11: Schematic representation of peripherin-2−MREG binding. The binding of MREG to the terminal five residues of human peripherin-2 is illustrated. MREG is colored purple and the peripherin-2 fusion domain yellow.

erin-2 binds mAb2B6 and prior to loading the polypeptide was shown to be biologically active, as defined by promotion of both membrane destabilization and model membrane fusion (data not shown). Therefore, we conclude that the value of $(5.61 \pm 1.27) \times 10^{-9}$ M is a more accurate reflection of the binding constant and MREG binds to peripherin-2 with high affinity. The decrease in affinity observed when MREG was immobilized was largely due to an increase in k_{off} (Table 3), indicating a destabilized heteromeric complex. The high affinity binding constant is consistent with the dose-dependent inhibition of fusion seen in Figure 3. Fusion of plasma membrane with disk membranes was inhibited with an IC_{50} of 1.5×10^{-6} M and with peripherin-2−ROM-1 enriched vesicles with an IC_{50} of 1.0×10^{-9} M. These data strongly suggest that the *in vitro* association between MREG and PerCter correlates with peripherin-2 functionality.

Using SPR technology, we found that MREG binds to the terminal 10 residues of peripherin-2 with a minimal requirement for the last five, as shown schematically in Figure 11. The specificity of binding to the C-terminus was confirmed in the GST pulldown analyses in which no binding was observed using GST−EC2 polypeptides or GST−ROM-1 C-terminal peptides. Of note is the lack of binding of MREG to a peripherin-2 polypeptide containing a scrambled helical

domain. This helical domain roughly corresponds to residues 309−329, not directly within the MREG binding domain. Although this region is not the MREG binding site, we predict that mutations of this region result in a structure that is either more intrinsically ordered, thus prohibiting folding-induced conformational changes, or more intrinsically disordered, thereby prohibiting MREG binding completely. NMR studies aimed at distinguishing between these two mechanisms are underway. Numerous studies of intrinsically disordered proteins suggest that structural disorder is functionally significant because it allows for increased plasticity in the regulation of multifunctional proteins (*65*−*67*). Advantages of such plasticity include an increased propensity to bind to several partners as well as an ability to overcome steric restrictions, thereby allowing for a larger surface for interactions between several different binding partners (*26*). Many IDPs undergo a transition to more ordered states or fold into stable secondary or tertiary structures upon binding to a physiological partner, a process termed induced folding, or coupled folding and binding (*36*). NMR studies conducted in our laboratory support a similar induced folding transition; PerCter becomes intrinsically more ordered through the formation of an α-helical domain in the presence of membrane mimetics.[2] In addition, more recent work in our laboratory demonstrates binding between calcium/calmodulin and peripherin-2 within this intrinsically disordered C-terminal domain.[3]

Since our goal was to understand how MREG alters peripherin-2 functionality, we assessed its role in membrane perturbing functions of peripherin-2. We have previously shown that peripherin-2 is a potent photoreceptor specific fusogen, with a C-terminal amphiphilic helical domain of residues Val^{311}−Leu^{325} (*20*, *21*) implicated in membrane fusion as well as targeting of peripherin-2 to *Xenopus* OS. Using a well-characterized cell free assay system designed to mimic *in vivo* photoreceptor specific fusion, MREG was shown to inhibit fusion between PM and two distinct target membranes, disk and peripherin-2−ROM-1 enriched vesicles. Moreover, when the MREG binding domain is deleted from the $Per^{\Delta 336-346}$ mutant, fusion with PM is enhanced. This enhancement is most likely due to the formation of a fusion competent conformation as reflected in the substantial decrease in fusion lag time observed with this mutant (Figure 7). Finally, the association of MREG with a peripherin-2−ROM-1 hetero-oligomeric complex has implications for peripherin-2-dependent trafficking and OS stability. Since MREG is localized to the IS and basal OS (Figures 9 and 10) and the site of disk morphogenesis and ROM-1 is required for OS viability and disk morphogenesis as illustrated in the ROM-1 knockout mouse (*68*), we propose that these two proteins may provide a regulatory mechanism for proper disk formation and disk closure during morphogenesis.

Finally, studies addressing how hydroxylamine treatment of disk membranes affects fusion provide insight into the mechanism of this regulation. Although MREG shows no sequence homology with any other protein, it contains a putative C-terminal palmitoylation site. While deacylation of MREG and membrane association was not addressed directly when disk membranes were stripped of loosely associated protein with the addition of HA, a substantial increase in the rate of fusion was observed, suggesting the removal of a fusion inhibitor. In add-back experiments, the addition of the supernatant fraction or pure MREG to the stripped disk membranes decreased the extent of fusion, suggesting that the fusion inhibitor had been restored. Therefore, we hypothesize that MREG is a transient fusion inhibitor with its regulatory role controlled by membrane association.

Given the multifunctional nature of peripherin-2, the formation of a peripherin-2−MREG complex may have other as yet undetermined consequences for photoreceptor viability and function. MREG may act as an additional linker protein between GARP and the cyclic GMP-gated channel. The tethering of GARP to peripherin-2 is predicted to result in a circular arrangement of the cGMP-gated channel, in juxtaposition to the disk rim. The distance of approximately 10 nm between the disk rim and the plasma membrane is not readily traversed if GARP assumes a globular conformation. Previous studies (*69*) suggest that GARP-1 and GARP-2 in their native state are intrinsically unfolded, thus allowing them to span most of this distance. In addition, these authors propose that a second as yet unidentified protein may help to fill the gap.

The terminal 10 residues of peripherin-2 make up part of the putative binding site(s) for both MREG and GARP (*69*). However, these two observations are in no way mutually exclusive when we consider the unique functional organization of disk components along the length of the outer segment. The OS contains multifunctional regions: OS base, site of new protein delivery and disk morphogenesis; mid-region, primary site of phototransduction; and OS tip, the site of disk packet formation and shedding. As is true of other disk membrane-associated proteins, peripherin-2 remains associated with a disk once assembled and travels up the length of the outer segment in that disk. Therefore, the idea that various protein components, both soluble and membrane-anchored, transiently bind to and associate with peripherin-2 at distinct regions along the OS remains intriguing and is supported by the serial tangential sectioning studies described here (Figure 9). Although not tested to date, the role of MREG as a regulator of membrane fusion processes is consistent with its effect on melanosome transfer and pigment incorporation (*35*). In melanocytes, the loss of MREG is postulated to alter melanosome phagocytosis, a process requiring fusion events (*34*).

Finally, these studies provide seminal evidence supporting a role for the peripherin-2−MREG complex in disk assembly. The two proteins colocalize within the inner segment and basal outer segment domains of the rod cell, in WT C57BL6 mice, with the MREG distribution apparently enriched in vesicle-like structures within the IS and connecting cilium. Double labeling experiments suggest that this vesicle population did not contain opsin (data not shown). While this is not shown directly in these studies, we postulate that the MREG-containing vesicles transport peripherin-2−ROM-1 complexes. The transport of these two rim specific proteins has been observed as being independent of opsin transport. In addition, Tam et al. (*19*) hypothesized that in transgenic *Xenopus* the transport of peripherin-2 likely required a protein cofactor. On the basis of its localization pattern and interactions with peripherin-2, MREG is a likely candidate.

ACKNOWLEDGMENT

We thank Dr. Muna Naash for providing GST−EC2 polypeptides as well as Drs. Michael Marks, Hydar Ali, and Bruce J. Shenker for providing primary cells and cell lines. We express our gratitude to Dr. B. J. Shenker for his expertise in generating the anti-MREG monoclonal antibodies and to Ms. Rosalina Espiritu for her expert technical assistance.

REFERENCES

1. Nguyen-Legros, J., and Hicks, D. (2000) Renewal of photoreceptor outer segments and their phagocytosis by the retinal pigment epithelium, *Int. Rev. Cytol. 196*, 245−313.
2. Connell, G. J., and Molday, R. S. (1990) Molecular cloning, primary structure, and orientation of the vertebrate photoreceptor cell protein peripherin in the rod outer segment disk membrane, *Biochemistry 29*, 4691−4698.
3. Molday, R. S., Hicks, D., and Molday, L. (1987) Peripherin. A rim-specific membrane protein of rod outer segment discs, *Invest. Ophthalmol. Visual Sci. 28*, 50−61.
4. Sanyal, S., and Hawkins, R. K. (1988) Development and degeneration of retina in rds mutant mice: Altered disk shedding pattern in the albino heterozygotes and its relation to light exposure, *Vision Res. 28*, 1171−1178.
5. Sanyal, S., Ruiter, A., and Hawkins, R. K. (1980) Development and degeneration of retina in rds mutant mice: Light microscopy, *J. Comp. Neurol. 194*, 193−207.
6. Hawkins, R. K., Jansen, H. G., and Sanyal, S. (1985) Development and degeneration of retina in rds mutant mice: Photoreceptor abnormalities in the heterozygotes, *Exp. Eye Res. 41*, 701−720.
7. Boesze-Battaglia, K., and Goldberg, A. F. (2002) Photoreceptor renewal: A role for peripherin/rds, *Int. Rev. Cytol. 217*, 183−225.
8. Sanyal, S., and Jansen, H. G. (1981) Absence of receptor outer segments in the retina of rds mutant mice, *Neurosci. Lett. 21*, 23−26.
9. Farjo, R., Skaggs, J. S., Nagel, B. A., Quiambo, A. B., Nash, Z. A., Fliesler, S. J., and Naash, M. I. (2006) Retention of function without normal disc morphogenesis occurs in cone but not rod photoreceptors, *J. Cell Biol. 173*, 59−68.
10. Stipp, C. S., Kolesnikova, T. V., and Hemler, M. E. (2003) Functional domains in tetraspanin proteins, *Trends Biochem. Sci. 28*, 106−112.
11. Ritter, L. M., Arakawa, T., and Goldberg, A. F. (2005) Predicted and measured disorder in peripherin/rds, a retinal tetraspanin, *Protein Pept. Lett. 12*, 677−686.
12. Goldberg, A. F., Moritz, O. L., and Molday, R. S. (1995) Heterologous expression of photoreceptor peripherin/rds and Rom-1 in COS-1 cells: Assembly, interactions, and localization of multisubunit complexes, *Biochemistry 34*, 14213−14219.
13. Goldberg, A. F. X., and Molday, R. S. (1996) Defective subunit assembly underlies a digenic form of retinitis pigmentosa linked to mutations in peripherin/rds and rom-1, *Proc. Natl. Acad. Sci. U.S.A. 93*, 13726−13730.
14. Goldberg, A. F., and Molday, R. S. (1996) Subunit composition of the peripherin/rds-rom-1 disk rim complex from rod photoreceptors: Hydrodynamic evidence for a tetrameric quaternary structure, *Proc. Natl. Acad. Sci. U.S.A. 35*, 6144−6149.
15. Goldberg, A. F., Loewen, C. J., and Molday, R. S. (1998) Cysteine residues of photoreceptor peripherin/rds: Role in subunit assembly and autosomal dominant retinitis pigmentosa, *Biochemistry 37*, 680−685.
16. Goldberg, A. F. X., Fales, L. M., Hurley, J. B., and Khattree, N. (2001) Folding and subunit assembly of photoreceptor peripherin/rds is mediated by determinants within the extracellular/intradiskal EC2 domain, *J. Biol. Chem. 276*, 42700−42706.
17. Loewen, C. J., and Molday, R. S. (2000) Disulfide-mediated oligomerization of peripherin/Rds and rom-1 in photoreceptor disk membranes. Implications for photoreceptor outer segment morphogenesis and degeneration, *J. Biol. Chem. 275*, 5370−5378.
18. Loewen, C. J., Moritz, O., and Molday, R. S. (2001) Molecular characterization of peripherin-2 and rom-1 mutants responsible for digenic retinitis pigmentosa, *J. Biol. Chem. 276*, 22388−22396.
19. Tam, B. M., Moritz, O. L., and Papermaster, D. S. (2004) The C terminus of peripherin/rds participates in rod outer segment targeting and alignment of disk incisures, *Mol. Biol. Cell. 15*, 2027−2037.
20. Boesze-Battaglia, K., Kong, F., Lamba, O. P., Stefano, F. P., and Williams, D. S. (1997) Purification and light dependant phosphorylation of a candidate fusion protein, photoreceptor peripherin/rds, *Biochemistry 36*, 6835−6846.
21. Boesze-Battaglia, K., Lamba, O. P., Napoli, A., Sinha, S., and Guo, Y. (1998) Fusion between retinal rod outer segment membranes and model membranes: A role for photoreceptor peripherin/rds, *Biochemistry 37*, 9477−9487.
22. Tam, B. M., Moritz, O. L., Hurd, L. B., and Papermaster, D. S. (2002) Characterization of the functional properties of the C-terminus of *Xenopus* peripherin, *Invest. Ophthalmol. Visual Sci. 43*, 2027.
23. Poetsch, A., Molday, L. L., and Molday, R. S. (2001) The cGMP-gated channel and related glutamic acid rich proteins interact with peripherin-2 at the rim region of rod photoreceptor disc membranes, *J. Biol. Chem. 276*, 48009−48016.
24. Boesze-Battaglia, K., Goldberg, A. F., Dispoto, J., Katragadda, M., Cesarone, G., and Albert, A. D. (2003) A soluble peripherin/Rds C-terminal polypeptide promotes membrane fusion and changes conformation upon membrane association, *Exp. Eye Res. 77*, 505−514.
25. Dyson, H. J., and Wright, P. E. (2005) Intrinsically unstructured proteins and their functions, *Nat. Rev. Mol. Cell Biol. 6*, 197−208.
26. Bowman, P., Galea, C. A., Lacy, E., and Kriwacki, R. W. (2006) Thermodynamic characterization of interactions between p27-(Kip1) and activated and non-activated Cdk2: Intrinsically unstructured proteins as thermodynamic tethers, *Biochim. Biophys. Acta 1764*, 182−189.
27. McNally, N., Kenna, P. F., Rancourt, D., Ahmed, T., Stitt, A., Colledge, W. H., Lloyd, D. G., Palfi, A., O'Neill, B., Humphries, M. M., Humphries, P., and Farrar, G. J. (2002) Murine model of autosomal dominant retinitis pigmentosa generated by targeted deletion at codon 307 of the rds-peripherin gene, *Hum. Mol. Genet. 11*, 1005−1016.
28. Sweet, H. O. (1983) Dilute suppressor, a new suppressor gene in the house mouse, *J. Hered. 74*, 305−306.
29. Moore, K. J. (1988) Dilute suppressor dsu acts semi-dominantly to suppress the coat color phenotype of a deletion mutant, dl20J, of the murine dilute locus, *Proc. Natl. Acad. Sci. U.S.A. 85*, 8131−8135.
30. Moore, K. J., Swing, D. A., Rinchik, E. M., Mucenski, M. L., Buchberg, A. M., Copeland, N. G., and Jenkins, N. A. (1988) The murine dilute suppressor gene dsu suppresses the coat-color phenotype of three pigment mutations that alter melanocyte morphology, d, ash and ln, *Genetics 119*, 933−941.
31. Moore, K. J., Swing, D. A., Copeland, N. G., and Jenkins, N. A. (1990) Interaction of the murine dilute suppressor gene (dsu) with fourteen coat color mutations, *Genetics 125*, 421−430; *126* (1), 285 (erratum).
32. Moore, K. J., Swing, D. A., Copeland, N. G., and Jenkins, N. A. (1994) The murine dilute suppressor gene encodes a cell autonomous suppressor, *Genetics 138*, 491−497.
33. Matesic, L. E., Yip, R., Reuss, A. E., Swing, D. A., O'Sullivan, T. N., Fletcher, C. F., Copeland, N. G., and Jenkins, N. A. (2001) Mutations in Mlph, encoding a member of the Rab effector family, cause the melanosome transport defects observed in leaden mice, *Proc. Natl. Acad. Sci. U.S.A. 98*, 10238−10243.
34. O'Sullivan, T. N., Wu, X. S., Rachel, R., Huang, J.-D., Swing, D. A., Matesic, L., Hammer, J. A., Copeland, N. G., and Jenkins, N. (2004) dsu functions in a MYO5A-independent pathway to suppress the coat color of dilute mice, *Proc. Natl. Acad. Sci. U.S.A. 101*, 16831−16836.
35. Seiberg, M. (2001) Keratinocyte-melanocyte interactions during melanosome transfer, *Pigment Cell Res. 14*, 236−242.
36. Cuomo, M., Nicotra, M. R., Apollonj, C., Fraioli, R., Giacomini, P., and Natali, P. G. (1991) Production and characterization of the murine monoclonal antibody 2G10 to a human T4-tyrosinase epitope, *J. Invest. Dermatol. 96*, 446−451.
37. Bennett, D. C., Cooper, P. J., Dexter, T. J., Devlin, L. M., Heasman, J., and Nester, B. (1989) Cloned mouse melanocyte lines carrying the germline mutations albino and brown: Complementation in culture, *Development 105*, 379−385.

38. Frangioni, J. V., and Neel, B. G. (1993) Solubilization and purification of enzymatically active glutathione S-transferase (pGEX) fusion proteins, *Anal. Biochem. 210*, 179−187.
39. Ding, X. Q., Stricker, H. M., and Naash, M. I. (2005) Role of the second intradiscal loop of peripherin/rds in homo and hetero associations, *Biochemistry 44*, 4897−4904.
40. Stefano, F. P., Krouse, J., Marta, P., and Boesze-Battaglia, K. (2002) Heterologous expression of WT and mutant photoreceptor peripherin/rds in Madin Darby canine kidney cells: An assessment of fusogenic function, *Exp. Eye Res. 74*, 267−283.
41. Shenker, B. J., Besack, D., McKay, T., Pankoski, L., Zekavat, A., and Demuth, D. (2004) *Actinobacillus actinomycetemcomitans* cytolethal distending toxin (Cdt): Evidence that the holotoxin is composed of three subunits: CdtA, CdtB, and CdtC, *J. Immunol. 172*, 410−417.
42. Lally, E., Kieba, I. R., Atsushi, S., Green, C. S., Rosenbloom, J., Korostoff, J., Wang, J., Shenker, B. J., Ortlepp, S., Robinson, M. K., and Billings, P. C. (1997) RTX toxins recognize a 2 integrin on the surface of human target cells, *J. Biol. Chem. 272*, 30463−30469.
43. Papermaster, D. S., and Dreyer, W. J. (1974) Rhodopsin content in the outer segment membranes of bovine and frog retinal rods, *Biochemistry 13*, 2438−2444.
44. Ovichinnikov, Y., Abdulaev, N. G., and Bogachuk, A. S. (1988) Two adjacent cysteine residues in the C-terminal cytoplasmic fragment of bovine rhodopsin are palmitylated, *FEBS Lett. 230*, 1−5.
45. Towbin, H., Staehelin, T., and Gordon, J. (1979) Electrophoretic transfer of proteins from polyacrylamide gels to nitrocellulose sheets: Procedure and some applications, *Proc. Natl. Acad. Sci. U.S.A. 76*, 4350−4354.
46. Wu, G., Krupnick, J. G., Benovi, J. L., and Lanier, S. M. (1997) Interaction of arrestins with intracellular domains of muscarinic and α-2 adrenergic receptors, *J. Biol. Chem. 272*, 17836−17842.
47. Boesze-Battaglia, K., Hennessey, T., and Albert, A. D. (1989) Cholesterol heterogeneity in bovine retinal rod outer segment disk membranes, *J. Biol. Chem. 264*, 8151−8155.
48. Boesze-Battaglia, K., Albert, A. D., and Yeagle, P. L. (1992) Fusion between disk membranes and plasma membranes of bovine photoreceptor cells is calcium dependent, *Biochemistry 31*, 3733−3737.
49. Boesze-Battaglia, K. (2000) Fusion between retinal rod outer segment membranes and model membranes: Functional assays and a role for peripherin/rds, *Methods Enzymol. 316*, 65−87.
50. Boesze-Battaglia, K., and Albert, A. D. (1989) Fatty acid composition of bovine retinal rod outer segment plasma membrane, *Exp. Eye Res. 49*, 699−701.
51. Hoekstra, D., Boer, T. D., Klappe, K., and Wilschut, J. (1984) Fluorescence method for measuring the kinetics of fusion between biological membranes, *Biochemistry 23*, 5675−5681.
52. Hoekstra, D., and Klappe, K. (1986) Sendai virus-erythrocyte membrane interaction: Quantitative and kinetic analysis of viral binding, dissociation and fusion, *J. Virol. 58*, 87−95.
53. Boesze-Battaglia, K., Stefano, F. P., Fenner, M., and Napoli, A. A., Jr. (2000) A peptide analogue to a fusion domain within photoreceptor peripherin/rds promotes membrane adhesion and destabilization, *Biochim. Biophys. Acta 1463*, 343−354.
54. Muller-Weeks, S., Boesze-Battaglia, K., and Fitzgerald, C. (2002) Deletional analysis of the rod photoreceptor cell peripherin/RDS carboxy-terminal region, *Exp. Eye Res. 75*, 143−154.
55. Moritz, O. L., and Molday, R. S. (1996) Molecular cloning, membrane topology, and localization of bovine rom-1 in rod and cone photoreceptor cells, *Invest. Ophthalmol. Visual Sci. 37*, 352−362.
56. Oprian, D. (1993) Expression of opsin genes in COS cells, in *Methods in Neuroscience* (Hargrave, P., Ed.) pp 301−306, Academic Press, San Diego.
57. Rattner, A., Smallwood, P. M., Williams, J., Cooke, C., Savchenko, A., Lyubarsky, A., Pugh, E. N., Jr., and Nathans, J. (2001) A photoreceptor-specific cadherin is essential for the structural integrity of the outer segment and for photoreceptor survival, *Neuron 32*, 775−786.
58. Liu, X., Vansant, G., Udovichenko, I. P., Wolfrum, U., and Williams, D. S. (1997) Myosin VIIa, the product of the Usher 1B syndrome gene, is concentrated in the connecting cilia of photoreceptor cells, *Cell Motil. Cytoskeleton 37*, 240−252.
59. Liu, X., Udovichenko, I. P., Brown, S. D., Steel, K. P., and Williams, D. S. (1999) Myosin VIIa participates in opsin transport through the photoreceptor cilium, *J. Neurosci. 19*, 6267−6274.
60. Sokolov, M., Strissel, K. J., Leskov, I. B., Michaud, N. A., Govardovskii, V. I., and Arshavsky, V. Y. (2004) Phosducin facilitates light-driven transducin translocation in rod photoreceptors, *J. Biol. Chem. 279*, 19149−19156.
61. Tam, B. M., Moritz, O. L., Hurd, L. B., and Papermaster, D. (2001) Are the COOH terminal regions for rod outer segment proteins potential targeting signals? *Invest. Ophthalmol. Visual Sci. 42*, (abstract).
62. Ritter, L., Boesze-Battaglia, K., Tam, B. M., Moritz, O., Khattree, N., Chen, S.-C., and Goldberg, A. F. (2004) Uncoupling of photoreceptor peripherin/rds C-terminal fusogenicity from biosynthesis, subunit assembly and targeting, *J. Biol. Chem. 279*, 39958−39967.
63. Connell, G. J., Bascom, R., Molday, L., Reid, D., McInnes, R., and Molday, R. S. (1991) Photoreceptor peripherin is the normal product of the gene responsible for retinal degeneration in the rds mouse, *Proc. Natl. Acad. Sci. U.S.A. 88*, 723−726.
64. Kaupp, U. B. (1995) Family of cyclic nucleotide gated ion channels, *Curr. Opin. Neurobiol. 5*, 434−442.
65. Obradovic, Z., Peng, K., Vucetic, S., Radivojac, P., Brown, C. J., and Dunker, A. K. (2003) Predicting intrinsic disorder from amino acid sequence, *Proteins 53* (Suppl. 6), 566−572.
66. Obradovic, Z., Peng, K., Vucetic, S., Radivojac, P., and Dunker, A. K. (2005) Exploiting heterogeneous sequence properties improves prediction of protein disorder, *Proteins 61* (Suppl. 7), 176−182.
67. Receveur-Brechot, V., Bourhis, J. M., Uversky, V. N., Canard, B., and Longhi, S. (2006) Assessing protein disorder and induced folding, *Proteins 62*, 24−45.
68. Clarke, G., Goldberg, A. F., Vidgen, D., Collins, L., Ploder, L., Schwarz, L., Molday, L., Rossant, J., Szel, A., Molday, R. S., Birch, D. G., and McInnes, R. R. (2000) Rom-1 is required for rod photoreceptor viability and the regulation of disk morphogenesis, *Nat. Genet. 25*, 67−73.
69. Batra-Safferling, R., Abarca-Heidemann, K., Korschen, H. G., Tziatzios, C., Stoldt, M., Budyak, I., Willbold, D., Schwalbe, H., Klein-Seetharaman, J., and Kaupp, U. B. (2006) Glutamic acid-rich proteins of rod photoreceptors are natively unfolded, *J. Biol. Chem. 281*, 1449−1460.

BI061466I